



Contents lists available at ScienceDirect

## Journal of Quantitative Spectroscopy &amp; Radiative Transfer

journal homepage: [www.elsevier.com/locate/jqsrt](http://www.elsevier.com/locate/jqsrt)

# Transcending the Rayleigh Hypothesis with multipolar sources distributed across the topological skeleton of a scatterer

Aristeidis G. Lamprianidis<sup>a,b,\*</sup>, Carsten Rockstuhl<sup>a,b,c</sup>, Ivan Fernandez-Corbaton<sup>c</sup>

<sup>a</sup> Institute of Theoretical Solid State Physics, Karlsruhe Institute of Technology, 76128, Karlsruhe, Germany

<sup>b</sup> Max Planck School of Photonics, Jena, 07745, Germany

<sup>c</sup> Institute of Nanotechnology, Karlsruhe Institute of Technology, Karlsruhe, 76021, Germany



## ARTICLE INFO

## Article history:

Received 29 September 2022

Revised 15 November 2022

Accepted 3 December 2022

Available online 8 December 2022

## Keywords:

Rayleigh hypothesis

Scattering theory

Topological skeleton

Discrete sources

Near-field

Multipolar representations

## ABSTRACT

There is an ever-growing need to study the optical response of complex photonic systems involving multi-scattering phenomena with strong near-field interactions. Since fully numerical methods often imply high computational costs, semi-analytical methods are preferred. However, most semi-analytical methods are commonly plagued by what is known as the problem of the Rayleigh Hypothesis: they typically use analytical representations of the scattered fields that are invalid in the near-field region of the scatterer. In this work, we present an alternative representation scheme for the scattered fields based on a distribution of multipolar sources across the topological skeleton of the scatterer. We demonstrate how such a representation overcomes the problem of the Rayleigh Hypothesis for scatterers of arbitrary geometry. In that regard, our work enriches the available toolkit of semi-analytical methods in light-scattering by pushing decisively against one of the fundamental limitations of the existing methods.

© 2022 The Author(s). Published by Elsevier Ltd.

This is an open access article under the CC BY license (<http://creativecommons.org/licenses/by/4.0/>)

## 1. Introduction

In 1907, Lord Rayleigh studied the diffraction of waves from gratings [1]. His famous hypothesis back then was that the reflected field by the grating could be represented everywhere above the grating –even inside the region of the corrugations– as a superposition of propagating and evanescent plane waves, propagating/decaying in discrete directions corresponding to the diffraction orders. This hypothesis was used to enforce the interface conditions at the surface of the grating to solve the diffraction problem. Since then, it has remained known in scientific history as the Rayleigh Hypothesis, and it has been imbued with a more generalized content that concerns the region of validity of analytical representations of fields. Initially constituting a topic of scientific dispute, the Rayleigh Hypothesis has been revisited multiple times from a mathematical, physical, or engineering point of view. Today, more than a century later, it remains an active topic of scientific research [2–24].

The first major mathematical treatment of the problem of the Rayleigh Hypothesis came several decades later when Millar highlighted the critical role of the analytic properties of the fields (i.e., related to their analytic continuation within the domain of

the scatterer) [2]. Since then, physicists and engineers have struggled to explicitly capitalize on the mathematical achievements and the state-of-the-art understanding of the problem. They also have been working to develop alternative practical methods to semi-analytically (i.e., not purely numerically) solve wave scattering problems that are not plagued with spurious effects related to the problem of the Rayleigh Hypothesis, as has usually been the case with the existing conventional methods.

Today, there is a growing need for the efficient simulation of complex photonic systems. Complex scattering phenomena are prominent in diverse research fields related to optical sensors [25,26], solar cells [27–30], optoelectronic devices such as light emitting diodes [31], disordered media [31,32], metamaterials [33,34], etc. Novel semi-analytical methods are being developed to efficiently simulate such complex photonic systems [35–43]. Quite often, the fully-numerical simulation of such systems, which are frequently characterized by a disparity of the involved optical length scales, can be expensive, if possible at all. Semi-analytical methods usually attempt to fill that gap. Their primary advantage is an analytical representation of the fields across an extended region of space. This enables the efficient semi-analytical modeling of complex wave interactions in the simulated

\* Corresponding author.

E-mail address: [aristeidis.lamprianidis@kit.edu](mailto:aristeidis.lamprianidis@kit.edu) (A.G. Lamprianidis).

system, which helps to reduce the computational burden tremendously. Therefore, it is evident that the problem of the Rayleigh Hypothesis, which is exactly related to the region of validity of the analytical representations of the fields, plays a pivotal role in all such semi-analytical methods since it directly affects their major advantage as a method.

A year after the seminal work of Lord Rayleigh, Gustav Mie solved the canonical problem of light scattering by a sphere [44]. As a representation of the scattered field, he employed a multipolar series where the origin was the center of the sphere. That constituted a natural representation for his case due to the geometry of the scatterer. However, the paradigm of Mie's representation still resonates today due to its strength. Today, we commonly keep employing the same representation Mie used to treat scatterers of non-spherical geometry [45,46]. However, here comes the devil of the Rayleigh Hypothesis indoors; it is known that such a representation is guaranteed to be valid only outside a sphere that circumscribes the scatterer.

Nevertheless, representations that unlock the access to the near-fields of the scatterers are essential for modeling multi-scattering phenomena involving scatterers placed in proximity, inside that problematic near-field region of each other. For example, modeling the electromagnetic coupling of nanoemitters such as molecules/quantum dots with nanoantennas or modeling the electromagnetic coupling of an array of tightly packed nanoparticles whose circumscribing spheres intersect with each other are further examples where semi-analytical modeling methods, employing Mie's conventional representation, usually fail to address the Rayleigh Hypothesis issue, which ends up posing as a fundamental challenge to the applicability of the method itself. Moreover, various semi-analytical methods exist for solving simpler scattering problems related to individual scatterers [47–50]. Enforcing correctly, in some way (frequently with a point-matching technique), the boundary conditions at the interface of the scatterer plays a central role in many of these methods. Hence, dealing with the problem of the Rayleigh Hypothesis, i.e., adopting representations for the fields whose region of validity includes the surface of the scatterers, is, again, of fundamental importance when it comes to the point of the semi-analytical method being functional.

The effects of the Rayleigh Hypothesis on conventional representations of the scattered fields have been explored. A plethora of methods employing alternative representations, usually based on a scheme with a spatial distribution of discrete sources, has been reported in the literature, including the Discrete Sources Method (DSM), the Null Field Method with Discrete Sources (NFM-DS), the Multiple Multipole Method (MMM), the Method of Auxiliary Sources (MAS), the Global Polarizability Matrix Method (GPM) [39,49,51–55]. Those alternative methods provided improved representation schemes that helped to model, with greater accuracy, the scattering from particles with extreme geometries in practice. They had their respective limitations, but, arguably, their most important problem was the lack of much evidence, maybe apart from intuition or some empirical rules [55], for the optimal placement of the discrete sources representing the scattered fields from a particle of arbitrary geometry.

In this work, we demonstrate that the distribution of multipolar sources across the topological skeleton of a scatterer constitutes a representation of the scatterer's field that transcends the problem of the Rayleigh Hypothesis, i.e., it can provide a valid representation of the fields everywhere outside the scatterer. The article is organized as follows: We begin with the theoretical statement and discussion of the problem of the Rayleigh Hypothesis. Then, we highlight the important aspects of the analytic properties of the fields before we introduce our proposed representation based on a distribution of sources across the topological skeleton of the scatterer, which constitutes a descriptor of its shape [56,57]. Fur-

thermore, we provide a numerical example with a comparison of the method against the conventional representation, demonstrate the advantages of the method, and discuss some related practical aspects. Finally, we discuss how our method can improve computational strategies in multi-scattering phenomena.

## 2. Theoretical treatment of the scattering problem of the Rayleigh Hypothesis

In this section, we will theoretically introduce the scattering problem of the Rayleigh Hypothesis. Afterwards, we briefly review the state-of-the-art treatment of the problem. Finally, we will approach it in our proposed way that helps to overcome the fundamental limitations of the Rayleigh Hypothesis. In particular, we will theoretically introduce a representation of the scattered fields based on multipolar sources distributed across the topological skeleton of the scatterer. This particular distribution grants access to the fields in the near-field region of the scatterer, which under conventional representation schemes is not the case.

### 2.1. Theoretical statement and discussion of the problem

Let us consider a surface  $S$  that may enclose the scatterer embedded in free space (see Fig. 1). An extension to the case of scatterers embedded in linear, isotropic, and homogeneous media is trivial. By making use of a Stratton-Chu-type integral [50,58,59] (see also Appendix A), we can represent the scattered field  $\mathbf{E}_{\text{sca}}$  (which we always consider being monochromatic) everywhere in the physical domain, i.e., in the free space  $V_{\text{Sout}}$  outside the surface  $S$ , in the following way:

$$\mathbf{E}_{\text{sca}}(\mathbf{r}) \equiv \int_S \vec{\mathbf{G}}(\mathbf{r}, \mathbf{r}_0) \cdot [\hat{\mathbf{n}}(\mathbf{r}_0) \times \nabla \times \mathbf{E}_{\text{sca}}(\mathbf{r}_0)] + \nabla \times \vec{\mathbf{G}}(\mathbf{r}, \mathbf{r}_0) \cdot [\hat{\mathbf{n}}(\mathbf{r}_0) \times \mathbf{E}_{\text{sca}}(\mathbf{r}_0)] d^2\mathbf{r}_0, \quad \mathbf{r} \in V_{\text{Sout}} \quad (1)$$

where  $\hat{\mathbf{n}}(\mathbf{r}_0)$  is the normal unit vector of  $S$  pointing inside  $V_{\text{Sout}}$  and  $\vec{\mathbf{G}}(\mathbf{r}, \mathbf{r}_0)$  is the Dyadic Green's Function (DGF) of the free space that gives the field induced at point  $\mathbf{r}$  from a unit point source placed at  $\mathbf{r}_0$ . Equation (1) constitutes a representation of the scattered field as the collective emission product of a radiating electric and magnetic surface current density distributed across the surface  $S$  of the scatterer.

However, following Morse & Feshbach, the DGF can be expanded in terms of the eigenmodes of the Helmholtz equation in free space [60]. This expansion offers alternative ways to represent the scattered fields with analytical expansions into such eigenmodes. The advantage of such representations is that they provide analytical access to the scattered fields into a big part of the physical domain  $V_{\text{Sout}}$ , which is rather beneficial when it comes to the analytical modeling of complex light-matter interactions. At the core of the Rayleigh Hypothesis is this region of validity of such analytical representations of the scattered fields. Dealing with the Rayleigh Hypothesis problematic practically means pushing the boundaries of the region of validity of such representations to include the whole physical domain  $V_{\text{Sout}}$ .

Let us further discuss the physics involved to elucidate the Rayleigh Hypothesis problematic better. There are eleven coordinate systems under which the monochromatic scalar Helmholtz equation in three dimensions is separable, with two introduced separation constants related to a couple of commuting symmetry operators in the enveloping algebra of the Helmholtz operator for each such coordinate system [60,61]. The three most common out of the eleven coordinate systems are the Cartesian, cylindrical, and spherical. Once employed to separate the homogeneous wave equation, they give its Cartesian, cylindrical, and spherical eigenmodes, which are the plane, cylindrical, and spherical waves,

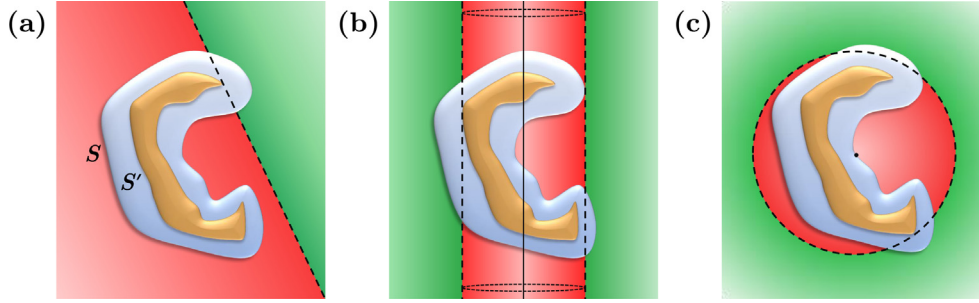


**Fig. 1.** The regions of validity of analytical representations of the scattered fields in terms of series of a) plane waves, b) cylindrical waves, and c) spherical waves. The scatterer is denoted with a grey color (bounded by surface  $S$ ). With brown color, we denote the region inside the scatterer that encloses all the singularities of the analytic continuation of the scattered field inside the scatterer (bounded by surface  $S'$ ). With green color, we denote the part of the physical domain where the representation is valid. The red color indicates the part of the physical domain where the representation is invalid. The domains of validity are bounded by a planar surface (a), or cylindrical surface (b), or spherical surface (c), that is indicated by the dashed lines above and is tangential to the singular surface  $S'$ , and is defined as  $\xi^{(3)} = \max\{\xi_s^{(3)}\}$  (see text). Representations based on expansions with respect to translated/rotated coordinate systems generally have an altered region of validity. (For interpretation of the references to colour in this figure legend, the reader is referred to the web version of this article.).

respectively. For those three cases, the corresponding commuting symmetry operators can be  $(P_x, P_y)$ ,  $(P_z, J_z)$ , and  $(\mathbf{J}^2, J_z)$ , respectively, with  $\mathbf{P}$  being the linear momentum operator and  $\mathbf{J}$  being the total angular momentum operator. If  $(\xi^{(1)}, \xi^{(2)}, \xi^{(3)})$  are the three coordinates of our coordinate system, the two commuting operators will be associated with two of those coordinates, let's say with  $\xi^{(1)}, \xi^{(2)}$  (see p.829 of [60]). For example, in the Cartesian coordinate system  $(x, y, z)$  the coordinates  $(x, y)$  are associated with the commuting symmetry operators  $(P_x, P_y)$ , whereas in the cylindrical coordinate system  $(\rho, \phi, z)$  the coordinates  $(\phi, z)$  are associated with the commuting symmetry operators  $(P_z, J_z)$ , and in the spherical coordinate system  $(r, \theta, \phi)$  the coordinates  $(\theta, \phi)$  are associated with the commuting symmetry operators  $(\mathbf{J}^2, J_z)$ .

For our purposes, the important thing to notice here is that due to the point singularity at  $\mathbf{r} = \mathbf{r}_0$ , the expansion of the DGF in terms of such eigenmodes becomes discontinuous across the surface that is defined by fixing the third coordinate  $\xi^{(3)}$ , i.e., the one that is not associated with the two commuting symmetry operators, to that of the respective coordinate of the position of the point source  $\xi_0^{(3)}$ . So, the representation of the DGF in terms of the eigenmodes of the homogeneous wave equation associated with the considered coordinate system will be discontinuous across the surface  $\xi^{(3)} = \xi_0^{(3)}$  (see Eq. 7.2.63 in [60]) and will take different forms for the two regions,  $\xi^{(3)} < \xi_0^{(3)}$  and  $\xi^{(3)} > \xi_0^{(3)}$ , so that the necessary condition for the regularity of the fields in all space apart from  $\mathbf{r} = \mathbf{r}_0$ , plus the radiation boundary conditions at infinity, are respected. Hence, we can expand the DGF in converging series of such plane, cylindrical, or spherical waves, although the convergence becomes poor due to the point singularity once we go close to the  $\xi^{(3)} = \xi_0^{(3)}$  surface. Such expansion will have the following branch-form:

$$\vec{\mathbf{G}}(\mathbf{r}, \mathbf{r}_0) \stackrel{\xi}{\equiv} \begin{cases} \sum_{\alpha, \xi_1, \xi_2} \vec{\mathbf{G}}_{\alpha, \xi_1, \xi_2}^-(\mathbf{r}, \mathbf{r}_0), & \xi^{(3)} < \xi_0^{(3)} \\ \sum_{\alpha, \xi_1, \xi_2} \vec{\mathbf{G}}_{\alpha, \xi_1, \xi_2}^+(\mathbf{r}, \mathbf{r}_0), & \xi^{(3)} > \xi_0^{(3)} \end{cases} \quad (2)$$

where we use the symbol  $\xi$  that takes the values (p, c, s) in order to refer to representations of the DGF in terms of expansions in plane, cylindrical, and spherical waves respectively. The expansion above involves a summation over the three eigenvalues with the two of them being  $\xi_1, \xi_2$ , i.e., the two eigenvalues that correspond to the two commuting symmetry operators of the  $\xi$ -coordinate system and the third one,  $\alpha$ , accounting for the vectorial nature of the eigenmodes, i.e., referring to the TE, TM modes where the electric (magnetic) field has no component along the vector that was used to construct the vectorial eigenmodes from the corre-

sponding scalar ones (see Eq. 13.1.6 in [60]). Let us note that the eigenvalues  $\xi_1, \xi_2$  may not be discrete and, in that case, the summation will be an integral over such continuous eigenvalue. For example, such is the case of the eigenvalues of the projection of the linear momentum operator  $\mathbf{P}$  on some axis. Note, also, that there is always a fourth eigenvalue, the wavenumber of the medium,  $k$ , corresponding to the operator  $\mathbf{P}^2$ . However, we suppress this eigenvalue for brevity reasons since it is fixed as long as we are considering monochromatic fields. Specific expressions of such expansions of the DGF in the  $\xi$ -eigenmode series are presented in Appendix B.

The problem of the Rayleigh Hypothesis becomes clear now. Assuming that the surface  $S$  of our scatterer is bounded by the two planes  $z = \min\{z_0\}$ ,  $z = \max\{z_0\}$ , or by the cylindrical surface  $\rho = \max\{\rho_0\}$ , or by the spherical surface  $r = \max\{r_0\}$ , then, in view of Eqs. (1), (2), we can see that, as long as we pick a single branch of the above expansion of the DGF, a representation of the scattered field in terms of series of plane waves guarantees access to the fields in the regions  $z > \max\{z_0\}$  (or  $z < \min\{z_0\}$ ). In contrast, a representation of the scattered field in terms of a series of cylindrical waves (with an origin corresponding to that of the coordinate system) guarantees access to the fields in the region  $\rho > \max\{\rho_0\}$  (i.e., outside the infinite cylinder that circumscribes the scatterer). Finally, a representation of the scattered field in terms of a series of spherical waves (again, with an origin corresponding to that of the coordinate system) guarantees access to the fields in the region  $r > \max\{r_0\}$  (i.e., outside the sphere that circumscribes the scatterer). Hence, these representations are only valid inside a part  $\tilde{V}_{\text{Sout}}$  of the physical domain  $V_{\text{Sout}}$ . The remaining part of the physical domain,  $V_{\text{Sout}} \setminus \tilde{V}_{\text{Sout}}$ , corresponds to a “restricted space” where the validity of our representation of the scattered field is not guaranteed. Consequently, a representation of the scattered field in terms of plane/cylindrical/spherical waves constitutes a natural choice for the case of planar/cylindrical/spherical-like scatterers, respectively, in the sense that it allows for a valid representation of the scattered fields in the biggest part of the embedding medium.

## 2.2. The role of the analytic properties of the scattered fields

Importantly, the analytic properties of the scattered fields have been at the core of the discussion involved around the Rayleigh Hypothesis problematic.

First of all, let us highlight that it is rather frequently the case that a series representation of the scattered field in terms of such  $\xi$ -eigenmodes that we described in the previous subsection provides access to some part of that “restricted volume”  $V_{\text{Sout}} \setminus \tilde{V}_{\text{Sout}}$ .

This implies that the above-mentioned boundaries are generally not the “hard boundaries” of the region of validity of such series representations. It has been mathematically shown that the position of the “hard boundaries” is related to the analytic properties of the scattered field [10]. Specifically, Kyurkchan et al. note in [9,10] the following: 1) The scattered field, being a solution of the Helmholtz equation, hence a ramifying analytic function, has a unique analytic continuation inside the non-physical domain up to a convex envelope inside  $S$  containing the singularities of the analytic continuation. 2) Such singularities of the analytic continuation of the scattered field inside  $S$  always exist since the scattered field is an analytic function that vanishes at infinity according to the radiation condition. 3) The position of the singularities inside  $S$  depends on the geometry of the surface  $S$  and on the position of potential singularities of the excitation source, which appear as image-singularities of the analytic continuation of the scattered field inside the volume of the scatterer. Such image-singularities may appear from the presence of singularities inside neighboring scatterers as well. This can render the task of locating the presence of singularities rather cumbersome and, most importantly, dependent on the actual scattering scenario in which the individual scatterer gets involved.

Two important concluding points have been highlighted by Kyurkchan et al. regarding the Rayleigh Hypothesis under the prism of the analytic continuation properties of the scattered fields [9,10].

The first point is that a series representation of the scattered field in terms of  $\xi$ -eigenmodes converges only in the region  $\xi^{(3)} > \max\{\xi_s^{(3)}\}$ , where  $\xi_s^{(3)}$  refers to the  $\xi^{(3)}$  coordinate of the singularities inside  $S$ . This is, in general, a less strict condition compared to the one that we had initially since for a smooth surface  $S$  we have that  $\max\{\xi_s^{(3)}\} < \max\{\xi_0^{(3)}\}$ . Actually, one of the first treatments of the original Rayleigh Hypothesis issue showed, by making use of conformal mapping transformations to study the analytic continuation properties of the fields, that the field that is diffracted by a sinusoidal grating with profile  $y = b\cos(kx)$ , can be represented everywhere in the physical domain -even inside the area of the corrugations- as a series of plane waves, only under the condition of  $kb < 0.448$ . Satisfying this condition corresponds to the case where all the singularities of the analytic continuation of the fields are located below the plane  $y = -b$  [2,5,10]. Recently, it has been demonstrated with numerical simulations that, for the case of spheroids, an expansion of the scattered field in terms of a series of spherical waves emanating from the origin of the scatterer is valid only outside the sphere circumscribing the two foci of the spheroid, instead of the whole spheroid [23,24]. And this is because the foci of the ellipse coincide with the singularities of the analytic continuation of the fields inside such a scatterer, as predicted by the above theory [9,10]. Let us also note here, though, another important thing that those numerical simulations revealed. When such series representations of the scattered field in  $\xi$ -eigenmodes finally fail to represent the fields with validity, they usually fail blatantly. The errors inside this “restricted volume” become orders of magnitude larger than the actual fields because there the series of the representation diverges due to the presence of the singularities [23,24]. This first point, highlighted by Kyurkchan et al., sheds light on the case of the Rayleigh Hypothesis that plagues representations of the scattered field based on a series of plane waves or a series of localized cylindrical/spherical waves (with fixed origin).

In Fig. 2, we illustrate the regions of validity of such representations of the scattered field for the three cases. It is important to note that such analytical expansions of the fields with respect to rotated/translated coordinate systems generally change the regions of validity of the representations of the scattered field. Along

this line, recently, there have been several attempts to circumvent the Rayleigh Hypothesis problematic by alternative round-about ways that involve an interplay of different representations of the scattered fields, i.e., employing expansions into eigen-waves with respect to appropriately translated/rotated coordinate systems. Specifically, in [62–64], an interplay between representations in terms of spherical and plane waves is used to access the fields inside the circumscribing sphere of the scatterers. In that case, modeling their coupling to planar interfaces or neighboring scatterers in close proximity becomes feasible. That work demonstrated that a plane wave representation of the scattered fields could unlock access to an arbitrarily oriented half-space tangential to the scatterer. Furthermore, in [65], an interplay between representations of the scattered field in terms of spherical waves with displaced origins was employed to move the spherical boundaries of the regions of validity of the representations arbitrarily. That allows for the solution of the scattering problem of a dimer of disks with high aspect ratios placed at closed proximity. Such approaches involve analytical transformations among the different representations employed to solve the scattering problem, and this, although analytically relatively trivial, numerically may be challenging [64]. In any case, such approaches to the problem of the Rayleigh Hypothesis avoid dealing with the core of the problem since they maintain problematic representations of the scattered fields that are not valid everywhere needed in the physical domain. Arguably, such an interplay between different field representations to access the fields into different sub-regions of the physical domain  $V_{\text{out}}$  (which allows for the proper treatment of different parts of the scattering problem) increases the complexity of the problem and may lead to unnecessary computational overhead also.

The second highlighted point is that an alternative integral representation of the scattered field in terms of radiation emanating from distributed current sources across a surface  $S'$  exists. Such representation provides full access to the fields in the entire physical domain  $V_{\text{out}}$ , as long as the support of the currents, i.e., surface  $S'$ , circumscribes all the singularities of the analytic continuation of the scattered field, and gets circumscribed by the surface of the scatterer,  $S$ , too. In Appendix A, we show how a current distribution over such a more compact (with which, in this work, we mean more compressed/economical) support of currents,  $S'$ , than the surface  $S$  where originally the current sources are distributed in the representation of Eq. (1), can be used to represent with validity the scattered field everywhere inside the physical domain. It has been numerically demonstrated in several cases that the semi-analytical methods on scattering problems, which adopt such an integral representation of the scattered field, have a stable performance only when the auxiliary radiating current sources are distributed over such a closed contour that circumscribes all the singularities of the analytic continuation of the fields inside the non-physical domain [10,66]. An algebraic theoretical framework that locates *a priori* the position of the shape-related singularities inside a scatterer of arbitrary geometry has been developed [9,10]. Computational methods such as MAS or MMM adopt such a representation scheme for the scattered field as the radiation emanating from distributed current sources over a surface  $S'$  inside the scatterer [55,67,68]. Initially, a substantial problem with these methods was the optimal placement of these auxiliary sources inside the scatterer. The analytic properties of the continuation of the fields inside the scatterer provided significant guidance in that regard. However, one could claim that, in practice, the scientific community has barely capitalized on this analysis so far, probably due to the mathematical complexity of the task of locating the singularities of the analytic continuation of the fields in the case of an arbitrary scattering problem. As we mentioned already, apart from the standard geometry-related singularities, extra image singularities related to the field exciting the scatterer may also exist. This

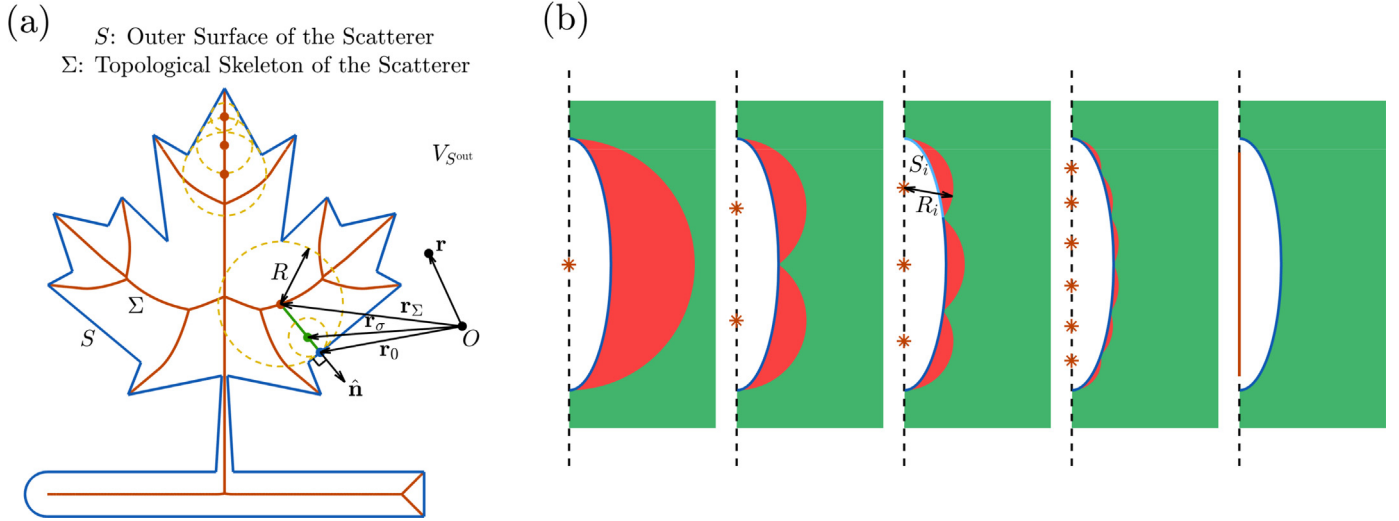


**Fig. 2.** Representations based on the topological skeleton of the scatterer: a) Illustration of the geometry of the problem in the 2D case, with the blue line being the outer surface of the scatterer  $S$  and with the red line being the topological skeleton of the scatterer  $\Sigma$  where the multipolar sources of the proposed representation of the scattered field are placed. b) The effect of the discretization of the topological skeleton of a prolate spheroid on the region of validity of the representation (green region). The cases of 1, 2, 3, and 6 origins of multipolar expansions (red stars) compared to the full topological skeleton, are illustrated. (For interpretation of the references to colour in this figure legend, the reader is referred to the web version of this article.)

would imply the need for varying representation schemes adapted each time to the scattering scenario that the scatterer gets involved in, which constitutes an undesired complication.

In what follows, we provide a general solution for the representation of the scattered fields that provides a path to overcome the problem of the Rayleigh Hypothesis while transcending such considerations of the analytic properties of the fields. Importantly, our method shall provide an all-around representation that can be employed to represent the fields radiated by a scatterer of *arbitrary geometry*, being involved in an *arbitrary scattering scenario*.

### 2.3. Introduction of the representation in terms of multipolar sources distributed across the topological skeleton of the scatterer

We need to take just a couple of small steps forward to tweak the integral representation of the scattered field already given by Eqs. (1), (2) and introduce a representation that is valid inside the whole physical domain  $V_{Sout}$ . Such a representation will be tailored to the arbitrary shape of the particular scatterer. It will provide a valid representation for any scattering scenario involving the particular scatterer while transcending the need for considerations related to the analytic properties of the fields.

The first step is to consider the following change of reference frame for the DGF, which consists of a shift of the origin of the multipolar sources by a displacement  $\mathbf{r}_\sigma(\mathbf{r}_0)$ , which depends on each  $\mathbf{r}_0$  point of the surface of the object:

$$\vec{\mathbf{G}}(\mathbf{r}, \mathbf{r}_0) = \vec{\mathbf{G}}(\mathbf{r} - \mathbf{r}_\sigma(\mathbf{r}_0), \mathbf{r}_0 - \mathbf{r}_\sigma(\mathbf{r}_0)), \quad (3)$$

where:

$$\mathbf{r}_\sigma(\mathbf{r}_0) = \mathbf{r}_0 - \hat{\mathbf{n}}(\mathbf{r}_0)R(\mathbf{r}_0)\sigma(\mathbf{r}_0), \quad (4)$$

with  $R(\mathbf{r}_0)$  being the radius of the largest circle (sphere) that can be inscribed inside  $S$ , without intersecting it, tangentially to point  $\mathbf{r}_0$ , and  $\sigma(\mathbf{r}_0)$  is some function that takes values within the range  $[0,1]$  (see Fig. 2a). Then, by introducing such a change of reference frame and using, also, exclusively the second branch of the expansion of the DGF of Eq. (2) in terms of either cylindrical waves (for 2D scatterers, translationally invariant along the  $z$ -axis) or spherical waves (for 3D scatterers), we get the following representation of the scattered field that is valid everywhere inside the physical

domain  $V_{Sout}$ :

$$\begin{aligned} \mathbf{E}_{sca}(\mathbf{r}) &\stackrel{\xi}{=} \sum_{\alpha, \xi_1, \xi_2}^{\xi} \int_S^{\xi} \mathbf{G}_{\alpha, \xi_1, \xi_2}^{\leftrightarrow+}(\mathbf{r} - \mathbf{r}_\sigma, \mathbf{r}_0 - \mathbf{r}_\sigma) \cdot [\hat{\mathbf{n}} \times \nabla \times \mathbf{E}_{sca}(\mathbf{r}_0)] \\ &\quad + \nabla \times \xi \mathbf{G}_{\alpha, \xi_1, \xi_2}^{\leftrightarrow+}(\mathbf{r} - \mathbf{r}_\sigma, \mathbf{r}_0 - \mathbf{r}_\sigma) \cdot [\hat{\mathbf{n}} \times \mathbf{E}_{sca}(\mathbf{r}_0)] d^2\mathbf{r}_0 \\ &= \sum_{\alpha, \xi_1, \xi_2}^{\xi} \int_S^{\xi} \mathcal{B}_{\alpha, \xi_1, \xi_2}^{\xi}(\mathbf{r}_0) \xi \mathbf{F}_{\alpha, \xi_1, \xi_2}^{(3)}(\mathbf{r} - \mathbf{r}_\sigma(\mathbf{r}_0)) d^2\mathbf{r}_0, \end{aligned} \quad (5)$$

for  $\mathbf{r} \in V_{Sout}$ ,

where  $\xi \mathcal{B}_{\alpha, \xi_1, \xi_2}^{\xi}(\mathbf{r}_0)$  are some complex amplitude coefficients that are to be calculated according to the formula above, and as  $\xi \mathbf{F}_{\alpha, \xi_1, \xi_2}^{(3)}(\mathbf{r} - \mathbf{r}_\sigma(\mathbf{r}_0))$  we denoted the spatial representation of either of the radiating Vector Cylindrical Harmonics (VCH), ( $\xi = c$ ), of Vector Spherical Harmonics (VSH), ( $\xi = s$ ), with origin at  $\mathbf{r} = \mathbf{r}_\sigma(\mathbf{r}_0)$ . Note that in the case of 2D scatterers, the surface integral above becomes a contour integral (see Appendix C for explicit expressions for the 2D and 3D cases). We ended up with a representation scheme of the scattered field in terms of a distribution of multipolar sources over a closed surface inside the scatterer. Let us highlight that the position of each such elementary source is determined according to Eq. (4) relevant to the position of a point  $\mathbf{r}_0$  on the surface  $S$  of the scatterer (see Fig. 2a), and that its amplitude  $\xi \mathcal{B}_{\alpha, \xi_1, \xi_2}^{\xi}(\mathbf{r}_0)$  is also directly specified by the values of the tangential electric and magnetic scattered fields at the same point  $\mathbf{r}_0$  on the surface  $S$  of the scatterer (see Eqs. (C.2) and (C.6)). However, even though we assign them such specific values here, it is important to note that those amplitudes are generally not unique (see Appendix A).

In this way, we have achieved a representation of the scattered field that is valid everywhere inside the physical domain  $V_{Sout}$ . And we achieved it by picking a representation for the individual radiation of each surface current  $[\hat{\mathbf{n}} \times \mathbf{E}_{sca}(\mathbf{r}_0)]$ ,  $[\hat{\mathbf{n}} \times \nabla \times \mathbf{E}_{sca}(\mathbf{r}_0)]$  at each point  $\mathbf{r}_0$  that is valid everywhere in  $V_{Sout}$ . And we achieved this by placing the center of the expansion of the DGF, which acts on those particular surface currents, somewhere on top of a linear segment inside the scatterer (see the green linear segment in Fig. 2a) that is the locus of the centers of all circles (spheres in the 3D case) that are tangent on  $S$  at  $\mathbf{r}_0$ , and that do not intersect  $S$  at any other point. In this case, the expansion of the second branch

of the employed DGF in Eq. (2) is valid everywhere in  $|\mathbf{r} - \mathbf{r}_\sigma| > |\mathbf{r}_0 - \mathbf{r}_\sigma|$ , and, hence, everywhere in  $V_{\text{Sout}}$ . By hiding in this way, at the interior of the scatterer, the surfaces where the branch of Eq. (2) lies for each individual surface current,  $|\mathbf{r} - \mathbf{r}_\sigma| = |\mathbf{r}_0 - \mathbf{r}_\sigma|$  (see the yellow dashed circles in Fig. 2a), we get a representation of  $\mathbf{E}_{\text{sca}}(\mathbf{r})$  that is valid everywhere in  $V_{\text{Sout}}$ . If the representation of the radiation of each surface current is valid everywhere in  $V_{\text{Sout}}$ , then so does the collective radiation emanating from all those surface currents, i.e., so does the representation that we use for the scattered field in Eq. (5).

Actually, Eq. (5) corresponds to a family of representations of the scattered field. That is because to each function  $\sigma(\mathbf{r}_0)$  corresponds a different representation with multipolar sources distributed over different surfaces inside the scatterer. In the limiting case that  $\sigma(\mathbf{r}_0) = 0, \forall \mathbf{r}_0$ , we have the sources distributed exactly across the surface of the scatterer  $S$ . This case corresponds to a representation equivalent to the representation used in classical surface integral methods [69]. The disadvantage of such an integral representation is that the kernel has singularities located across the surface  $S$ . This results in a poor convergence of the fields' representation when the observation point  $\mathbf{r}$  comes close to  $S$ , i.e., in the vicinity of the scatterer. However, we can push the singularities of the kernel further inside the scatterer by letting  $\sigma(\mathbf{r}_0)$  take non-zero values. Specifically, taking the other limiting case of  $\sigma(\mathbf{r}_0) = 1, \forall \mathbf{r}_0$ , we end up with a representation that is based on multipolar sources distributed across the surface  $\Sigma$ , which is defined as:  $\mathbf{r}_\Sigma(\mathbf{r}_0) = \mathbf{r}_\sigma(\mathbf{r}_0)|_{\sigma(\mathbf{r}_0)=1, \forall \mathbf{r}_0}$ . This zero-volume-enclosing surface,  $\Sigma$ , is by definition the *topological skeleton* of the scatterer (see Fig. 2a).

The topological skeleton (also known as the medial axis) of an object is defined as the locus of the centers of circles (spheres in 3D) that are tangent to its outer surface at two or more points, where all such circles (spheres in 3D) are contained inside the object [57]. It was initially introduced by Blum in 1967 as a tool for biological shape recognition [56]. The medial axis, together with the associated radius function of the maximally inscribed circles (spheres in 3D), which we denote as  $R(\mathbf{r}_0)$ , is called the medial axis transform (MAT) of the object. The MAT is a complete shape descriptor, meaning it can be used to reconstruct the shape of the original object. So, in that sense, it constitutes a compressed way to encode the shape of the object. Apart from medical imaging applications, the topological skeleton has found a wide variety of applications in fields such as computer graphics, animation, visualization, digital inspection, computer design, pattern recognition, robotics, collision detection, etc., where a compact shape representation supporting shape analysis and synthesis is important [57]. It is a quite mature field of research, and several methods exist to calculate the topological skeleton of a given object, with Voronoi diagrams usually playing a central role in that regard [70–72].

From the physical point of view, on the one hand, we can claim that the introduced topological-skeleton-based representation of the fields constitutes an optimal representation since it provides the locus of the most compact support of multipolar sources able to overcome the problem of the Rayleigh Hypothesis for an arbitrary scattering scenario involving the considered scatterer. Let us highlight that the topological skeleton does not necessarily pass through the singularities of the analytic continuation of the scattered fields, yet it provides a representation of the scattered field that is valid everywhere in  $V_{\text{Sout}}$  (see Eq. (5) above). As we demonstrate in Appendix A, if we would assume the *a priori* knowledge of the analytic properties of the scattered fields, then the most optimal and compact representation that does not suffer from the problem of the Rayleigh Hypothesis, would, instead, be the one based on a distribution of multipolar sources across the topological skeleton of the surface  $S'$ , inside  $S$ , that encloses all the singularities of the analytic continuation of the fields inside the scatterer.

On the other hand, by placing the multipolar sources on the topological skeleton  $\Sigma$ , we also managed to move the singularities of the representation of the scattered field as far away from the surface of the scatterer  $S$  as possible. In that sense, this is the optimal placement of the distribution of the sources among all cases of different  $\sigma(\mathbf{r}_0)$ , guaranteeing better convergent properties of the near-fields. However, as it can be seen in Fig. 2a, the topological skeleton  $\Sigma$  touches the surface of the scatterer  $S$  at its sharp edges; such points always host singularities. This is not the case for a smooth surface  $S$  (which, in this work, we generally consider it to be).

Importantly, let us note that not all parts of the topological skeleton are equally significant. On the one hand, significant small parts can be responsible for the radiation of a big part of the surface currents. Take, for example, a sphere whose topological skeleton is a single point at its center. That point can host the origin of a multipolar series that validly represents the fields all over the physical domain  $V_{\text{Sout}}$ . On the other hand, it is also possible that large parts of the topological skeleton correspond to only a minor part of the radiating surface currents. In such a case, we could “prune” such insignificant parts of the topological skeleton to attain a more compact representation of the fields. This comes at the cost of sacrificing the guaranteed access to a valid representation of the fields at a small enough region of the physical domain in the vicinity of the scatterer.

Equation (5) describes an infinite-dimensional representation of the scattered fields that allows us to transcend the problem of the Rayleigh Hypothesis. However, for practical purposes, we need to render that representation finite-dimensional. This means that the integral in Eq. (5) should be replaced by a finite sum. This implies the discretization of the topological skeleton  $\Sigma$  and its substitution by a set of  $N$  points that act as centers of multipolar expansions for the field that is radiated by the surface currents distributed over a surface  $S_i$ , that is part of  $S = \sum_{i=1}^N S_i$ . Specifically, for a finite-dimensional representation of the scattered field with multipolar sources distributed over the discretized topological skeleton, we can write:

$$\begin{aligned} \mathbf{E}_{\text{sca}}(\mathbf{r}) &\stackrel{\xi}{=} \sum_{\alpha, \xi_1, \xi_2} \sum_{i=1}^N \int_{S_i} \xi \mathbf{G}_{\alpha, \xi_1, \xi_2}^{\leftrightarrow+}(\mathbf{r} - \mathbf{r}_i, \mathbf{r}_0 - \mathbf{r}_i) \cdot [\hat{\mathbf{n}} \times \nabla \times \mathbf{E}_{\text{sca}}(\mathbf{r}_0)] \\ &\quad + \nabla \times \xi \mathbf{G}_{\alpha, \xi_1, \xi_2}^{\leftrightarrow+}(\mathbf{r} - \mathbf{r}_i, \mathbf{r}_0 - \mathbf{r}_i) \cdot [\hat{\mathbf{n}} \times \mathbf{E}_{\text{sca}}(\mathbf{r}_0)] d^2\mathbf{r}_0 \\ &= \sum_{\alpha, \xi_1, \xi_2} \sum_{i=1}^N \xi \mathcal{B}_{\alpha, \xi_1, \xi_2, i} \xi \mathbf{F}_{\alpha, \xi_1, \xi_2}^{(3)}(\mathbf{r} - \mathbf{r}_i), \\ &\quad \text{for } |\mathbf{r} - \mathbf{r}_i| > R_i, \forall i \end{aligned} \quad (6)$$

with  $\xi \mathcal{B}_{\alpha, \xi_1, \xi_2, i}$  being some complex amplitudes. See Appendix C for explicit expressions for the 2D and 3D cases.

The above expression is only valid outside the union of circles (spheres in 3D) that are centered at  $\mathbf{r} = \mathbf{r}_i$  and have a radius of  $R_i$  that is large enough to contain inside each circle (sphere in 3D) the surface current sources that are distributed over the surface  $S_i$  (highlighted with light blue color in Fig. 2b) that is associated with the  $i$ th center of multipolar expansion of the discretized topological skeleton. In Fig. 2b, we illustrate the effect of discretization of the topological skeleton of a prolate spheroid on the region of validity of the representation of the scattered fields. By increasing the number of points of expansion employed, i.e., by increasing the dimensionality of the representation, we unlock access to the near-fields closer and closer to the surface of the scatterer  $S$ . For example, already with six centers of multipolar expansion, we can see that we have reduced the problematic near-field region (with red color in Fig. 2b) rather significantly. The full topological skeleton of a prolate spheroid of semi-minor axis  $a$  and semi-major axis  $b$  (along  $z$ ) is a linear segment connecting the points

$(x, y, z) = (0, 0, \pm(b^2 - a^2)/b)$ . Let us note that those two points are not the foci of the spheroid, which are singular points of the analytic continuation of the scattered fields inside a prolate spheroid [9,10,23,24].

We want to emphasize three things. First, the surface bounding the union of spheres defined by  $|\mathbf{r} - \mathbf{r}_i| = R_i$  does not constitute a hard boundary for the region of validity of the representation of the scattered fields. The hard boundary is expected to be the surface bounding a union of spheres defined by  $|\mathbf{r} - \mathbf{r}_i| = R'_i$ . Here,  $R'_i \leq R_i$ .  $R'_i$  shall be the radius of the smallest sphere that encloses all the singularities of the analytic continuation of the fields that are radiated by the surface current sources distributed over the surface  $S_i$ .

Second, let us note that the region of validity of the finite-dimensional representation of the scattered fields that we introduced is not unique since the amplitudes  ${}^\xi B_{\alpha, \xi_1 \xi_2, i}$  are not unique. Specifically, an arbitrary and non-optimal assignment of the radiating surface currents to the  $N$  multipolar centers of expansion (which, let us consider fixed here), may still lead, on the one hand, to multipolar amplitudes that can represent the far-field but, on the other hand, may obstruct the access to the near-fields.

Finally, let us note that the maximum multipolar order of the sources placed at  $\mathbf{r} = \mathbf{r}_i$  needed to accurately represent the fields emanating from the corresponding radiating surface currents distributed over  $S_i$  shall depend on the radius  $R_i$ . Points of the topological skeleton placed at a large optical distance from the surface of the scatterer  $S$  generally require a larger number of multipoles for their expansions compared to points closer to  $S$ . We will discuss the effects of the multipolar truncations in further detail in the following section.

### 3. Numerical demonstration of the topological skeleton method

In this section, we demonstrate the performance of the method of the topological skeleton numerically. We explore how it deals with the problem of the Rayleigh Hypothesis and how it provides a valid representation of the near-field of a scatterer.

In our indicative example, we use as a scatterer an axially symmetric object with the complex shape of a seahorse. In Fig. 3, the white-shaded region indicates the cross-section of such a scatterer along a meridian plane. We consider the scatterer to be circumscribed by a sphere of radius half the wavelength of light in free space ( $\lambda$ ). The scatterer is embedded in free space and made of an isotropic, non-magnetic material with a refractive index of  $n = 3.477$ . We consider the excitation of the scatterer by a monochromatic, TE-polarized regular VSH of angular momentum along the  $z$ -axis,  $\mu = 0$ , and multipolar order,  $\nu = 2$  [see Eq. (B.10) for its definition]. We perform a full-wave numerical simulation with a finite element solver JCM-suite [73] to record the electromagnetic response of the scatterer under such excitation. By exploiting the axial symmetry of both the geometry and the excitation, we performed the simulations in two dimensions, and we were able to reach an accuracy of the recorded near-fields up to at least the fourth significant digit. We used finite elements of size  $\lambda/50$  and polynomial order 10. We recorded the scattered field within the near-field zone, inside a sphere of radius  $0.65\lambda$  containing the scatterer. The norm of the scattered field,  $|\mathbf{E}_{\text{sca}}(\mathbf{r})|$ , that we recorded from the full-wave simulation is plotted in Fig. 3a.

Next, we want to study and compare how the problem of the Rayleigh Hypothesis is manifested in that particular example, once we employ different analytical representation schemes to reconstruct the simulated target scattered field. For this, we record the tangential field components at 6000 points on the contour of the surface of the scatterer across a meridian plane, and we use them to get the complex amplitudes of the different analytical represen-

tations that we compare. For this, we establish the following logarithmic relative error metric:

$$\mathcal{E}(\mathbf{r}) = \log_{10} \left[ \frac{|\mathbf{E}_{\text{sca}}^{\text{analytical}}(\mathbf{r}) - \mathbf{E}_{\text{sca}}^{\text{numerical}}(\mathbf{r})|}{|\mathbf{E}_{\text{sca}}^{\text{numerical}}(\mathbf{r})|} \right]. \quad (7)$$

First, we consider the conventional representation of the scattered field based on a single center of multipolar expansion at  $\mathbf{r} = 0$ . Specifically, we use Eq. (C.8) to get the amplitudes of the representation of the scattered field in terms of a series of radiating VSHs centered at  $\mathbf{r} = 0$  (magenta star in Fig. 3b). As discussed already, such a representation of the fields is expected to be valid outside the minimal sphere that circumscribes the scatterer ( $r > \max\{r_0\}$ ). We use the numerically calculated amplitudes of the series expansion of the fields to reconstruct them analytically by making use of Eq. (C.7) and calculate the log. relative error  $\mathcal{E}(\mathbf{r})$  by comparing them against the numerical results. In Fig. 3b, we show color plots of  $\mathcal{E}(\mathbf{r})$  for increasing multipolar order of truncation of the infinite series ( $\nu_{\text{max}}$ ). The dashed magenta line denotes the spherical shell of  $r = \max\{r_0\}$ , inside of which the Rayleigh Hypothesis is expected to get violated. Indeed, we observe that, for  $\nu_{\text{max}} = 10$ , we barely have any errors recorded in the dark blue region outside of the magenta sphere. Actually, the errors are small, even a bit inside that sphere. As we discussed already, the hard boundary of validity of such a representation is not the magenta sphere but a sphere of a generally smaller radius that circumscribes all the singularities of the analytic continuation of the scattered field inside the region of the scatterer. It is important to observe that by increasing  $\nu_{\text{max}}$ , on the one hand, we achieve better and better convergence of the series representation of the fields closer and closer to that spherical shell enclosing the singularities. But, on the other hand, we get a worse and worse divergence of the series representation of the fields in the physical domain contained inside the spherical shell that encloses the singularities. Such divergence of the fields has already been observed in References [23,24]. Here, whereas, for  $\nu_{\text{max}} = 1$ , we observe a relative error of an order of magnitude larger than the norm of the scattered near-field, for  $\nu_{\text{max}} = 10$ , we observe a relative error of twelve orders of magnitude larger than the norm of the scattered near-field.

Such large errors may at first suggest that the existing semi-analytical method of multiple light scattering, based on such conventional multipolar representations of the fields in terms of localized series of VSHs, would always become useless for modeling the near-field coupling between closely placed scatterers. In practice, this is not strictly the case, however. In Ref. [24], it was shown, with counterexamples featuring near-field interactions between dimers of prolate spheroids, that sufficiently convergent results can be obtained in unexpected near-field regions when a very large number (40) of multipolar contributions is considered (increasing the dimensionality of the problem dramatically, though). Eventually, this additionally requires that the calculations are performed with quadruple-precision arithmetic to account for the interactions between multipoles of high order properly. Those results seem to suggest that the problem of the Rayleigh Hypothesis within the context of multi-scattering calculations is not intrinsic, i.e., associated with the inherently problematic analytic properties of the adopted representations of the fields. Instead, it appears to be a problem of numerical nature if we are always able to get convergent solutions for the general multi-scattering problem associated with an arbitrary geometric setup by ever increasing the multipolar truncation order and the arithmetic precision used for the calculations. However, on the one hand, whether this suggestion is true in its generality remains an interesting open question, and, on the other hand, even in such a case, it is evident that such problematic numerical issues stem from the analytic aspects of the

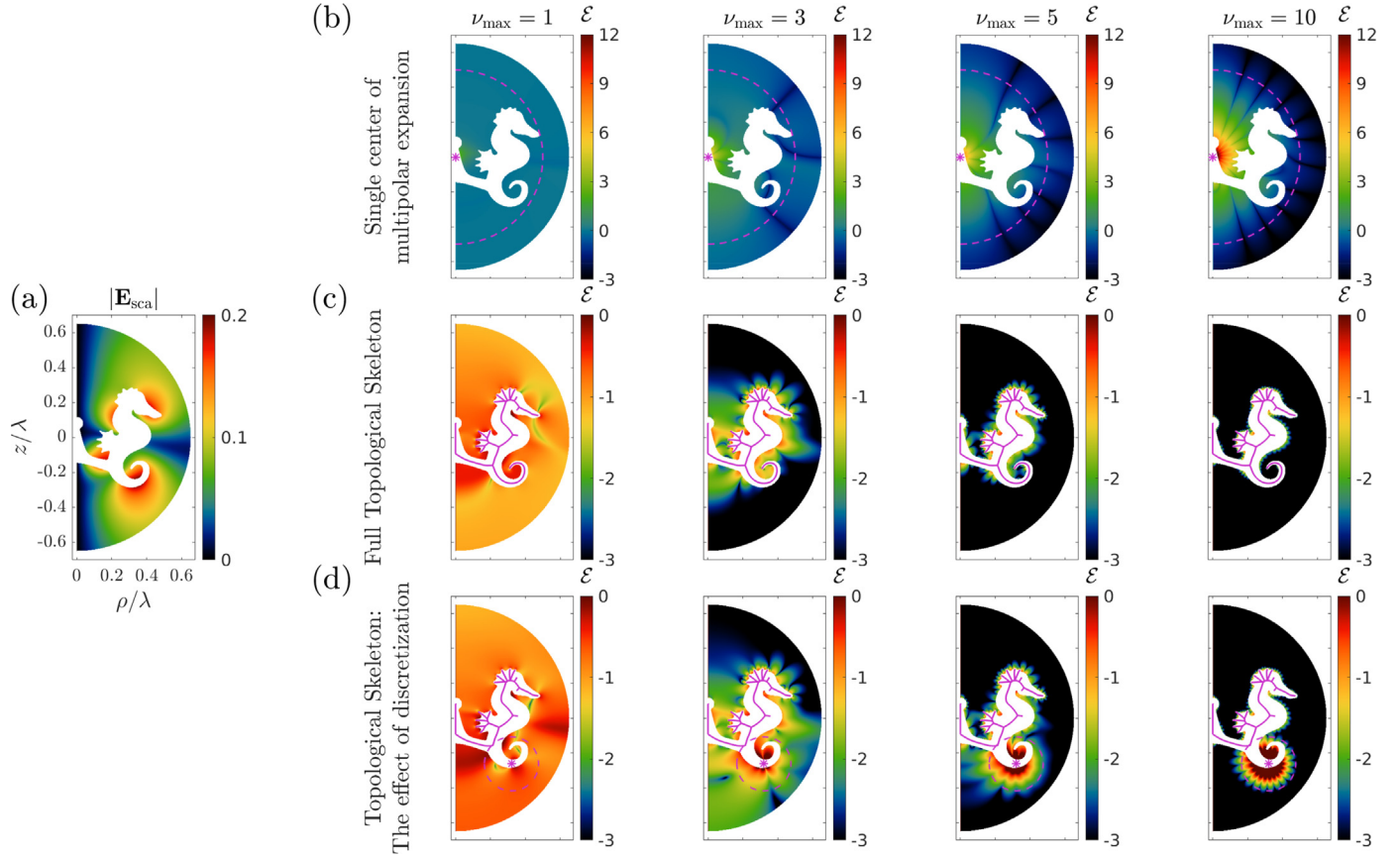


**Fig. 3.** Numerical example with a comparison of the performance of different analytical representations of the scattered field, elucidating their relation with the problem of the Rayleigh Hypothesis. a) Plot of the norm of the scattered near-field of a sub-wavelength, axially symmetric seahorse (with its cross-section along a meridian plane being white-shaded) excited by a regular VSH, as it was calculated by a finite element solver. Plots of the logarithmic relative error,  $\epsilon$ , in the representation of the scattered near fields by: b) the conventional case of a single center of multipolar expansion of the fields (magenta star), c) a distribution of multipolar sources across the entire topological skeleton of the seahorse (magenta line), d) a distribution of multipolar sources across the topological skeleton of the seahorse with its tail being truncated and substituted by a single origin of multipolar expansion (magenta star) to represent the radiation of the tail specifically. The plots are given for different truncation orders,  $\nu_{max}$ , of the infinite multipolar sums. The dashed magenta circles in (b) and (d) indicate the theoretical regions of validity of the representations. We can see how the representation of the topological skeleton allows for the transcendence of the problem of the Rayleigh Hypothesis that plagues the conventional representation of the fields.

problem. We highlight that the method presented in this paper provides representations of the scattered field that converge everywhere outside the scatterers for general geometries and that require only a reasonable number of multipoles. In the next section, we discuss how our method can be used to improve computational strategies for multi-scattering phenomena.

Next, we consider the newly introduced representation scheme, which is based on a distribution of multipolar sources over the topological skeleton of the scatterer, to represent the scattered fields. We first construct the topological skeleton of the axially symmetric seahorse based on a constrained Delaunay Triangulation method [72] (see the magenta solid line in Fig. 3c for a cross-section of the topological skeleton of the seahorse along a meridian plane). Then, we use Eq. (C.8) to get the amplitudes  $\xi B_{\alpha, \xi_1 \xi_2, i}$  and represent the scattered field in terms of radiating VSHs distributed over the topological skeleton of the seahorse with Eq. (C.7). We densely discretize the meridian cross-section of the topological skeleton using  $N = 6000$  points, i.e., we assign each considered elementary radiating surface current to a distinct center of multipolar expansion. The integration over the azimuthal dimension of the skeleton is performed adaptively, resembling a perfectly fine discretization along the azimuthal dimension. In Fig. 3c, we plot again the calculated log. relative errors of the considered representation scheme for increasing multipolar order for the truncation of the series. We can observe that, by  $\nu_{max} = 10$ , an accuracy of more than three significant digits is achieved almost all over the near-field

region we monitor. Actually, already by  $\nu_{max} = 3$ , we get an acceptable convergence of the series representation of the fields. The topological skeleton method can fully transcend the problem of the Rayleigh Hypothesis. Let us note again that the closer the observation point to the surface of the scatterer, the larger the number of multipoles needed for an accurate representation of the fields.

Finally, we consider another representation scheme for the scattered fields to study the discretization effects of the topological skeleton method. Specifically, as in the previous case, we begin with the full topological skeleton of the seahorse, but now we truncate its tail and employ a single center of multipolar expansion to represent the radiating fields emanating from the surface currents distributed over the tail of the seahorse. The magenta star in Fig. 3d denotes that introduced center of multipolar expansion. Due to the axial symmetry, note that the star represents a ring of multipolar sources rather than a single multipolar center. Interestingly, DSM commonly employs multipolar sources placed in the complex plane that constitute the image of such a ring of sources in the real space [49]. Again, we use Eq. (C.8) to get the amplitudes  $\xi B_{\alpha, \xi_1 \xi_2, i}$  of our new representation. Now, the dimensionality of the representation is reduced to  $N = 4451$ , as we truncated 1550 points belonging to the tail of the skeleton of the seahorse and substituted them with a single origin of expansion. It is expected that the representation provides access to the near-fields everywhere outside a torus centered at the magenta star and circumscribing the truncated tail of the seahorse. The dashed ma-

genta circle in Fig. 3d indicates a cross-section of this torus along a meridian plane where we plot a map of the calculated log. relative errors  $\mathcal{E}(\mathbf{r})$  again. Indeed, we can observe that such a representation still provides great accuracy of the reconstructed fields everywhere outside the aforementioned torus (actually, everywhere outside the torus -of a bit smaller radius- that circumscribes the singularities of the analytic continuation of the fields radiated by the truncated tail of the seahorse). Therefore, in practice, we can significantly reduce the dimensionality of the topological-skeleton-based representation of the fields to a small enough number of centers of multipolar expansions by sacrificing the access of the representation to a small enough near-field region in the vicinity of the scatterer. For example, we saw in Fig. 2b that only six properly placed centers of multipolar expansion already provide a good representation of the scattered fields by a prolate spheroid with an aspect ratio of three. Nevertheless, more complicated geometries generally require representations of higher dimensionality.

We want to emphasize the following two key observations regarding the number of multipoles needed for sufficient convergence of the aforementioned multipolar series representations of the scattered field: 1) the smaller the optical distance between the observation point and the spherical (cylindrical in 2D) shell enclosing the singularities of the analytic continuation of the field represented by the particular multipolar center of expansion, and 2) the larger the optical distance between the multipolar center of expansion and the aforementioned singular shell, i.e., the larger the radius of the shell, the more multipoles are needed for the convergence of the series representation of the field. Let us note that this implies quite significant limitations for methods based on dipolar-only representations, such as e.g., in [39]. Such representations can only be practically applicable either for cases of scatterers that are sufficiently optically small or for distributions of dipolar sources that are placed at close enough optical distances from the surface of the scatterer [this would correspond, for example, to the non-optimal case of the representation of Eq. (5) with small values of  $\sigma(\mathbf{r}_0)$ ], which would typically increase the dimensionality of the representation significantly, though, since it would generally require the spatial distribution of a larger number of centers of expansion.

In Appendix D, we provide three figures as additional support for the above-mentioned observations on the convergence of the scattered field representations based on infinite multipolar series.

#### 4. Improving multi-scattering computational strategies with the topological skeleton method

Our contribution paves the way toward the efficient semi-analytical modeling of complex optical systems comprised of large ensembles of particles and characterized by strong near-field coupling. Fully numerical methods of analyzing such systems are computationally rather demanding, and semi-analytical methods have proved to be useful in that regard. Our findings are pushing decisively against the limitations that the existing semi-analytical methods traditionally face concerning the problem of the Rayleigh Hypothesis, i.e., concerning the problematic representation of the near-fields of the scatterers. Specifically, our introduced topological-skeleton-based representation of the radiated fields provides clear and general guidelines for the proper placement of the sources in existing semi-analytical scattering methods based on discrete sources, freeing them from the fundamental problem of the Rayleigh Hypothesis [39,49,51–55].

Numerical methods, such as in References [39,45,46], can be generalized to calculate the T-matrices of scatterers of arbitrary geometry, by making use of our introduced topological-skeleton-based representation of the scattered fields. However, apart from a proper basis for representing the scattered fields, there is also

a crucial need to represent the incident field properly. In a multi-scattering scenario, the effective incident field on each scatterer, including the scattered fields from the rest of the scatterers, also possesses singularities in its analytic continuation in the near-field region of the scatterer, which also affect the region of convergence of the representations. Adopting a representation of the incident field that is based on a series of regular VSHs centered at the same origins of expansion on the topological skeleton that are used for the radiating multipolar sources of the scattered field provides a means to represent the incident field accurately everywhere within the scatterer. Each center of expansion has a different spherical region of convergence, and the union of all those regions encloses the whole domain of the scatterer under the condition that the analytic continuation of the effective incident field possesses no singularities inside a surface  $S_{i/o}$  enclosing, e.g., the red volume in Fig. 2b, which encloses the scatterer. As a result, being able to represent the incident field properly everywhere over such a surface  $S_{i/o}$ , we can use Eq. (A.5), in the absence of external sources inside  $S_{i/o}$ , and expand the tangential surface currents using the same multipolar series representation to end up with a topological-skeleton-based series representation of the incident field, whose amplitudes are associated with the tangential surface currents of the incident field on  $S_{i/o}$ . Such a representation of the incident field can also be employed as a basis for the new topological-skeleton-based T-matrix. The latter can then be used to model multi-scattering phenomena with strong near-field coupling, whose study, previously, has been problematic by conventional semi-analytical methods due to the problem of the Rayleigh Hypothesis. As long as there is, in general, a guaranteed convergent representation of both the incident and scattered fields of each arbitrary scatterer inside and outside its input/output surface  $S_{i/o}$  respectively, then the multi-scattering method should be computationally stable.

#### 5. Final remarks

In this work, we focused on the problem of the Rayleigh Hypothesis as it is commonly manifested in semi-analytical methods of solving wave scattering problems that are based on, frequently problematic in the near-field region, analytical representations of the radiated field from scatterers with complex geometries. We discussed how the problem of the Rayleigh Hypothesis could plague such methods, and we proposed an alternative representation of the fields, based on sources distributed over the topological skeleton of the scatterer, that is demonstratively able to transcend the problem of the Rayleigh Hypothesis. We also studied some practical aspects of the implementation of the proposed method and discussed how it can be used to improve computational strategies for multi-scattering phenomena.

We want to note that, although in this work we only deal with the representations of the scattered field, i.e., with the exterior problem, the Rayleigh Hypothesis issue may also exist for the interior problem, i.e., there is always a need for valid representations of the field induced inside the scatterer, as well. The induced field also has singularities in its analytic continuation outside the scatterer, which may plague its representation [74]. For example, the Extended Boundary Condition Method (EBCM) is said to disregard the Rayleigh Hypothesis. Still, it does employ, however, a particular representation of the field induced inside the scatterer based on a series of localized regular VSHs to apply the boundary conditions and solve the scattering problem [50]. This does assume, though, that such a series representation of the induced fields is convergent across the whole surface of the scatterer. And because such is not generally the case, this can be the reason that the method fails to solve the scattering problem in the case of scatterers with high aspect ratios, for example. Improved representation schemes

of the fields induced inside the scatterer that were based on discrete sources have been employed by several methods to practically deal with that manifestation of the problem of the Rayleigh Hypothesis for the case of the interior problem [49,51–53,75]. Finally, we would like to note that, even though our analysis was formulated in the context of the scattering of electromagnetic waves, the key ideas also apply to the scattering of acoustic waves, for which a similar method can be readily developed.

### Declaration of Competing Interest

The authors declare that they have no known competing financial interests or personal relationships that could have appeared to influence the work reported in this paper.

### CRediT authorship contribution statement

**Aristeidis G. Lamprianidis:** Conceptualization, Methodology, Investigation, Writing – original draft. **Carsten Rockstuhl:** Writing – review & editing, Project administration. **Ivan Fernandez-Corbaton:** Writing – review & editing, Supervision.

### Data availability

Data will be made available on request.

### Acknowledgments

A.G.L., and C.R. are part of the Max Planck School of Photonics, supported by the Bundesministerium für Bildung und Forschung, the Max Planck Society, and the Fraunhofer Society. A.G.L. acknowledges support from the Karlsruhe School of Optics and Photonics (KSOP). C.R. acknowledges support by the German Research Foundation through Germany's Excellence Strategy via the Excellence Cluster 3D Matter Made to Order (EXC-2082/1 - 390761711) and the Carl Zeiss Foundation through the "Carl-Zeiss-Focus@HEiKA". I.F.C., and C.R. acknowledge support by the Helmholtz Association via the Helmholtz program Materials Systems Engineering (MSE).

### Appendix A. Stratton-Chu-type integral representations of the scattered field

Stratton-Chu-type integral representations of the scattered fields are a classic [50,58–60]. Here, in this Appendix, we will derive Eq. (1) of the main text and discuss further related details.

The derivation of Stratton-Chu-type integral representations always begins with employing the Green's vector identity in its differential form:

$$\begin{aligned} & \mathbf{P} \cdot (\nabla \times \nabla \times \mathbf{Q}) - \mathbf{Q} \cdot (\nabla \times \nabla \times \mathbf{P}) \\ &= \nabla \cdot [\mathbf{Q} \times (\nabla \times \mathbf{P}) - \mathbf{P} \times (\nabla \times \mathbf{Q})], \end{aligned} \quad (\text{A.1})$$

where  $\mathbf{P}, \mathbf{Q}$  are some vector fields. For our purposes, we choose them to be the electric field  $\mathbf{E}(\mathbf{r}_0)$  and the Dyadic Green's Function (DGF)  $\vec{\mathbf{G}}(\mathbf{r}, \mathbf{r}_0)$  of the background medium, respectively. Those satisfy the following monochromatic wave equations in linear, lossless, isotropic, and homogeneous media:

$$(\nabla \times \nabla \times - k^2)\mathbf{E}(\mathbf{r}_0) = i\omega\mu_0\mathbf{J}(\mathbf{r}_0), \quad (\text{A.2})$$

$$(\nabla \times \nabla \times - k^2)\vec{\mathbf{G}}(\mathbf{r}, \mathbf{r}_0) = \vec{\mathbf{I}}\delta(\mathbf{r} - \mathbf{r}_0), \quad (\text{A.3})$$

where  $k$  is the wavenumber of the medium,  $\omega$  is the frequency of the waves,  $\mu_0$  is the magnetic permeability of the medium,  $\mathbf{J}(\mathbf{r}_0)$  is the electric current density hosted in the medium,  $\vec{\mathbf{I}}$  is the identity matrix, and  $\delta$  is the Dirac-delta function. Doing this substitution in Eq. (A.1), integrating both sides over a closed volume  $V_0$  bounded

by a surface  $S_0$ , and applying the Gauss's theorem, finally gives the following main result:

$$\begin{aligned} \mathbf{E}(\mathbf{r})\delta(\mathbf{r} \in V_0) &= i\omega\mu_0 \int_{V_0} \vec{\mathbf{G}}(\mathbf{r}, \mathbf{r}_0) \cdot \mathbf{J}(\mathbf{r}_0) d^3\mathbf{r}_0 \\ &+ \int_{S_0} \vec{\mathbf{G}}(\mathbf{r}, \mathbf{r}_0) \cdot [\hat{\mathbf{n}}(\mathbf{r}_0) \times \nabla \times \mathbf{E}(\mathbf{r}_0)] \\ &+ \nabla \times \vec{\mathbf{G}}(\mathbf{r}, \mathbf{r}_0) \cdot [\hat{\mathbf{n}}(\mathbf{r}_0) \times \mathbf{E}(\mathbf{r}_0)] d^2\mathbf{r}_0, \end{aligned} \quad (\text{A.4})$$

where  $\delta(\mathbf{r} \in V_0)$  takes the value 1 for  $\mathbf{r} \in V_0$  and the value 0 otherwise, and  $\hat{\mathbf{n}}(\mathbf{r}_0)$  is the unit vector normal to the surface  $S_0$  and that points towards the interior of  $V_0$ . We also made use of the vector identity:  $\mathbf{a} \cdot (\mathbf{b} \times \mathbf{c}) = (\mathbf{a} \times \mathbf{b}) \cdot \mathbf{c}$ . Equation (A.4) can be used to derive several integral representations in scattering theory.

First of all, by applying Eq. (A.4) for the case of the infinite background medium that is involved in the scattering problem and integrating over an arbitrary volume  $V_0$  bounded by  $S_0$ , we can get the following integral representation of the incident field inside  $V_0$  as a sum of a volume integral term involving fields by sources hosted inside  $V_0$ , and another surface integral term that is related to an electromagnetic field radiated from sources outside of  $V_0$ :

$$\begin{aligned} \mathbf{E}_{\text{inc}}(\mathbf{r})\delta(\mathbf{r} \in V_0) &= \mathbf{E}_{\text{inc,inside}}(\mathbf{r}) + \mathbf{E}_{\text{inc,outside}}(\mathbf{r}) \\ &= i\omega\mu_0 \int_{V_0} \vec{\mathbf{G}}(\mathbf{r}, \mathbf{r}_0) \cdot \mathbf{J}(\mathbf{r}_0) d\mathbf{r}_0^3 \\ &+ \int_{S_0} \vec{\mathbf{G}}(\mathbf{r}, \mathbf{r}_0) \cdot [\hat{\mathbf{n}}(\mathbf{r}_0) \times \nabla \times \mathbf{E}_{\text{inc}}(\mathbf{r}_0)] \\ &+ \nabla \times \vec{\mathbf{G}}(\mathbf{r}, \mathbf{r}_0) \cdot [\hat{\mathbf{n}}(\mathbf{r}_0) \times \mathbf{E}_{\text{inc}}(\mathbf{r}_0)] d^2\mathbf{r}_0. \end{aligned} \quad (\text{A.5})$$

Let us now derive Eq. (1) of the main text. For this, first we will make use of Eq. (A.4) for the case of the total fields,  $\mathbf{E}_{\text{tot}}(\mathbf{r}) = \mathbf{E}_{\text{inc}}(\mathbf{r}) + \mathbf{E}_{\text{sca}}(\mathbf{r})$ , that are defined inside the space  $V_{\text{Sout}}$  that is bounded by the surface of the scatterer  $S$  and some spherical surface at infinity  $S_\infty$ . This gives that:

$$\begin{aligned} \mathbf{E}_{\text{tot}}(\mathbf{r})\delta(\mathbf{r} \in V_{\text{Sout}}) &= i\omega\mu_0 \int_{V_{\text{Sout}}} \vec{\mathbf{G}}(\mathbf{r}, \mathbf{r}_0) \cdot \mathbf{J}(\mathbf{r}_0) d\mathbf{r}_0^3 \\ &+ \int_{S+S_\infty} \vec{\mathbf{G}}(\mathbf{r}, \mathbf{r}_0) \cdot [\hat{\mathbf{n}}(\mathbf{r}_0) \times \nabla \times \mathbf{E}_{\text{tot}}(\mathbf{r}_0)] \\ &+ \nabla \times \vec{\mathbf{G}}(\mathbf{r}, \mathbf{r}_0) \cdot [\hat{\mathbf{n}}(\mathbf{r}_0) \times \mathbf{E}_{\text{tot}}(\mathbf{r}_0)] d^2\mathbf{r}_0. \end{aligned} \quad (\text{A.6})$$

Then, by making use of the far-field expressions of the scattered fields (see Eqs. (2.94,2.95) in [50]), together with the far-field expression of the DGF and its curl (see Eqs. (8.55,8.57) in [76]), we can prove that:

$$\begin{aligned} & \vec{\mathbf{G}}(\mathbf{r}, \mathbf{r}_0) \cdot [\hat{\mathbf{n}}(\mathbf{r}_0) \times \nabla \times \mathbf{E}_{\text{sca}}(\mathbf{r}_0)] \\ &+ \nabla \times \vec{\mathbf{G}}(\mathbf{r}, \mathbf{r}_0) \cdot [\hat{\mathbf{n}}(\mathbf{r}_0) \times \mathbf{E}_{\text{sca}}(\mathbf{r}_0)] = 0, \end{aligned} \quad (\text{A.7})$$

for  $r \ll r_0, \mathbf{r}_0 \in S_\infty$ .

Finally, by making use of Eq. (A.5) both for  $S_0 = S$  and  $S_0 = S_\infty$  (considering that there are no current sources inside the space of the scatterer,  $V_{\text{Sin}}$ , that is bounded by  $S$ ), and combining those results together with Eqs. (A.6,A.7), we readily get Eq. (1) of the main text, as well as the following Stratton-Chu formula:

$$\begin{aligned} \left. \begin{aligned} -\mathbf{E}_{\text{inc}}(\mathbf{r})\delta(\mathbf{r} \in V_{\text{Sin}}) \\ \mathbf{E}_{\text{sca}}(\mathbf{r})\delta(\mathbf{r} \in V_{\text{Sout}}) \end{aligned} \right\} &= \int_S \vec{\mathbf{G}}(\mathbf{r}, \mathbf{r}_0) \cdot [\hat{\mathbf{n}}(\mathbf{r}_0) \times \nabla \times \mathbf{E}_{\text{tot}}(\mathbf{r}_0)] \\ &+ \nabla \times \vec{\mathbf{G}}(\mathbf{r}, \mathbf{r}_0) \cdot [\hat{\mathbf{n}}(\mathbf{r}_0) \times \mathbf{E}_{\text{tot}}(\mathbf{r}_0)] d^2\mathbf{r}_0. \end{aligned} \quad (\text{A.8})$$

Note that in the above integral, we consider that  $\mathbf{n}$  points towards the interior of  $V_{\text{Sout}}$ , and hence this minus in front of  $\mathbf{E}_{\text{inc}}(\mathbf{r})$  gets introduced.

In view of the second branch of the last equation, together with Eq. (1) of the main text, we can deduce that such an integral representation of the scattered field is not unique. Apart from the electric and magnetic surface current distributions,  $[\hat{\mathbf{n}}(\mathbf{r}_0) \times \nabla \times \mathbf{E}_{\text{sca}}(\mathbf{r}_0)]$ ,  $[\hat{\mathbf{n}}(\mathbf{r}_0) \times \mathbf{E}_{\text{sca}}(\mathbf{r}_0)]$ , there is a big family of current distributions over the surface of the scatterer  $S$ ,  $[\hat{\mathbf{n}}(\mathbf{r}_0) \times \nabla \times \mathbf{E}_{\text{tot}}(\mathbf{r}_0)]$ ,  $[\hat{\mathbf{n}}(\mathbf{r}_0) \times \mathbf{E}_{\text{tot}}(\mathbf{r}_0)]$ , that are able to generate the same scattered fields  $\mathbf{E}_{\text{sca}}(\mathbf{r})$  in  $V_{\text{Sout}}$ . This is because, the surface currents  $[\hat{\mathbf{n}}(\mathbf{r}_0) \times \nabla \times \mathbf{E}_{\text{inc}}(\mathbf{r}_0)]$ ,  $[\hat{\mathbf{n}}(\mathbf{r}_0) \times \mathbf{E}_{\text{inc}}(\mathbf{r}_0)]$  that correspond to an incident field that has no singularities inside the region of the scatterer, demonstrate zero contribution to the fields radiated in  $V_{\text{Sout}}$  through the DGF in the Stratton-Chu integral representation. In that sense, it is important to highlight that the amplitudes  ${}^\xi \mathcal{B}_{\alpha, \xi_1 \xi_2}(\mathbf{r}_0)$  of the representation in Eq. (5) of the main text are not unique.

Finally, let us discuss how the knowledge of the analytic properties of the scattered field can further modify the integral representation of Eq. (1). Let us assume that we know that all the singularities, branch points, of the analytic continuation of the function of the scattered field  $\mathbf{E}_{\text{sca}}(\mathbf{r})$  are enclosed inside a surface  $S'$ , that is enclosed inside the surface of the scatterer  $S$ . Then, we can proceed in the same way that we derived Eq. (1), but now integrating over  $S'$  instead of  $S$ , and, due to the analytic continuation of  $\mathbf{E}_{\text{sca}}(\mathbf{r})$  inside the volume bounded by  $S$  and  $S'$  (which practically means the analytic continuation of the solution of the Helmholtz equation of the scattered field inside that "unphysical" domain), we can get the following formula:

$$\mathbf{E}_{\text{sca}}(\mathbf{r})\delta(\mathbf{r} \in V_{\text{Sout}}) \equiv \int_{S'} \vec{\mathbf{G}}(\mathbf{r}, \mathbf{r}_0) \cdot [\hat{\mathbf{n}}(\mathbf{r}_0) \times \nabla \times \mathbf{E}_{\text{sca}}(\mathbf{r}_0)] + \nabla \times \vec{\mathbf{G}}(\mathbf{r}, \mathbf{r}_0) \cdot [\hat{\mathbf{n}}(\mathbf{r}_0) \times \mathbf{E}_{\text{sca}}(\mathbf{r}_0)] d^2\mathbf{r}_0, \quad (\text{A.9})$$

where  $V_{\text{Sout}}$  is the volume outside the surface  $S'$  (bounding the brown domain in Fig. 1), and where we also assume the knowledge of the analytic continuation of the scattered field on  $S'$ . In that sense,  $S'$  constitutes the most compact support of radiating currents that can reconstruct the scattered field everywhere inside the physical domain  $V_{\text{Sout}} \in V_{\text{Sout}}$ . Hence, assuming the *a priori* knowledge of the analytic properties of the scattered fields, we can claim that the most optimal representation of the scattered fields shall be based on multipolar sources distributed across the topological skeleton, not of surface  $S$ , but of surface  $S'$ , instead. Nevertheless, as we discuss in the main text, such a representation, being tailored to the particular analytic properties of the fields, cannot be generalized for an arbitrary scenario involving the scatterer since the surface  $S'$  generally varies because of the image singularities induced by the arbitrary field that may excite the scatterer.

## Appendix B. Analytical expansions of the Dyadic Green's Function of free space in terms of the Cartesian, cylindrical, spherical eigenmodes of the Helmholtz equation

The Dyadic Green's Function  $\vec{\mathbf{G}}(\mathbf{r}, \mathbf{r}_0)$  of an infinite, linear, lossless, isotropic, and homogeneous medium obeys the monochromatic wave equation given in Eq. (A.3). Following [60], the DGF can be expanded into a series of eigenmodes of the homogeneous wave equation of its corresponding medium. The three most common expansions we also use in the main part of the article are the ones into plane, cylindrical, and spherical waves. We will call those eigenmodes as Vector Planar/Cylindrical/Spherical Harmonics (VPHs/VCHs/VSHs), respectively. We will denote their spatial representation as  ${}^\xi \mathbf{F}(\mathbf{r})$ . The symbol  $\xi$  takes the values p, c, s to refer to the planar/cylindrical/spherical case, respectively. The eigenmodes can be constructed from the solutions of the monochromatic, scalar homogeneous wave equation expressed in the corresponding coordinate system. As mentioned in the main text, those

scalar modes are eigenstates of two symmetry operators. Therefore, apart from the wavenumber of the medium  $k$ , they will also depend on two other eigenvalues. For these three coordinate systems those scalar eigenmodes  ${}^\xi \psi(\mathbf{r})$  are given by:

$${}^p \psi_{k_x k_y}^{(\pm)}(x, y, z) = e^{i(k_x x + k_y y \pm \sqrt{k^2 - k_x^2 - k_y^2} z)}, \quad (\text{B.1})$$

$${}^c \psi_{\mu k_z}^{(\iota)}(\rho, \phi, z) = Z_\mu^{(\iota)}(\tilde{\rho}) e^{i\mu\phi} e^{ik_z z}, \quad (\text{B.2})$$

$${}^s \psi_{\mu\nu}^{(\iota)}(r, \theta, \phi) = \gamma_{\mu\nu} z_\nu^{(\iota)}(kr) P_\nu^\mu(\cos\theta) e^{i\mu\phi}, \quad (\text{B.3})$$

where  $k_x, k_y, k_z$  are the eigenvalues of the projection of the linear momentum operator along the  $x$ -,  $y$ -,  $z$ -axis, respectively. Moreover,  $k_\rho(k_x, k_y) = \sqrt{k_x^2 + k_y^2}$ .  $\mu$  is the eigenvalue of the projection of the total angular momentum operator along the  $z$ -axis and  $\tilde{\rho} = k_\rho(k_z)\rho$  with  $k_\rho(k_z) = \sqrt{k^2 - k_z^2}$ .  $\nu(\nu+1)$  is the eigenvalue of the total angular momentum squared operator.  $Z_\mu^{(\iota)}(x)$  denotes the cylindrical Bessel ( $\iota=1$ ) and Hankel ( $\iota=3$ ) functions of the first kind, of order  $\mu$ , whereas  $z_\nu^{(\iota)}(x)$  denotes the spherical Bessel ( $\iota=1$ ) and Hankel ( $\iota=3$ ) functions of the first kind, of order  $\nu$ .  $P_\nu^\mu(x)$  are the associated Legendre functions of the first kind and  $\gamma_{\mu\nu} = \sqrt{\frac{(2\nu+1)(\nu-\mu)!}{4\pi\nu(\nu+1)(\nu+\mu)!}}$  are some normalization coefficients.

When following [60], we can construct a full set of divergent-free vectorial eigenmodes based on the above scalar eigenmodes. We will use the symbol  $\alpha$  to denote the TE ( $\alpha=M$ ) and TM ( $\alpha=N$ ) such modes.

The VPHs  ${}^p \mathbf{F}_{\alpha, k_x k_y}^{(\pm)}(\mathbf{r})$ , will be given by the formulas below:

$${}^p \mathbf{F}_{M, k_x k_y}^{(\pm)}(\mathbf{r}) \triangleq \frac{1}{k_\rho} \nabla \times \left[ \hat{\mathbf{z}} {}^p \psi_{k_x k_y}^{(\pm)}(x, y, z) \right] = -i \hat{\phi}_{\mathbf{k}}(k_x, k_y) {}^p \psi_{k_x k_y}^{(\pm)}(x, y, z), \quad (\text{B.4})$$

$${}^p \mathbf{F}_{N, k_x k_y}^{(\pm)}(\mathbf{r}) \triangleq \frac{1}{k} \nabla \times \left[ {}^p \mathbf{F}_{M, k_x k_y}^{(\pm)}(\mathbf{r}) \right] = -\hat{\theta}_{\mathbf{k}}^{(\pm)}(k_x, k_y) {}^p \psi_{k_x k_y}^{(\pm)}(x, y, z), \quad (\text{B.5})$$

where:

$$\hat{\phi}_{\mathbf{k}}(k_x, k_y) = \frac{-k_y \hat{\mathbf{x}} + k_x \hat{\mathbf{y}}}{k_\rho}, \quad (\text{B.6})$$

$$\hat{\theta}_{\mathbf{k}}^{(\pm)}(k_x, k_y) = \pm \frac{\sqrt{k^2 - k_\rho^2}}{kk_\rho} (k_x \hat{\mathbf{x}} + k_y \hat{\mathbf{y}}) - \frac{k_\rho}{k} \hat{\mathbf{z}}. \quad (\text{B.7})$$

The VCHs,  ${}^c \mathbf{F}_{\alpha, \mu k_z}^{(\iota)}(\mathbf{r})$ , will be given by the formulas below:

$${}^c \mathbf{F}_{M, \mu k_z}^{(\iota)}(\mathbf{r}) \triangleq \frac{1}{k_\rho} \nabla \times \left[ \hat{\mathbf{z}} {}^c \psi_{\mu k_z}^{(\iota)}(\rho, \phi, z) \right] = e^{ik_z z} e^{i\mu\phi} \left[ i\mu \frac{Z_\mu^{(\iota)}(\tilde{\rho})}{\tilde{\rho}} \hat{\rho} - \frac{\partial Z_\mu^{(\iota)}(\tilde{\rho})}{\partial \tilde{\rho}} \hat{\phi} \right], \quad (\text{B.8})$$

$${}^c \mathbf{F}_{N, \mu k_z}^{(\iota)}(\mathbf{r}) \triangleq \frac{1}{k} \nabla \times \left[ {}^c \mathbf{F}_{M, \mu k_z}^{(\iota)}(\mathbf{r}) \right] = e^{ik_z z} e^{i\mu\phi} \times \left[ i \frac{k_z}{k} \frac{\partial Z_\mu^{(\iota)}(\tilde{\rho})}{\partial \tilde{\rho}} \hat{\rho} - \mu \frac{k_z}{k} \frac{Z_\mu^{(\iota)}(\tilde{\rho})}{\tilde{\rho}} \hat{\phi} + \frac{k_\rho}{k} Z_\mu^{(\iota)}(\tilde{\rho}) \hat{\mathbf{z}} \right]. \quad (\text{B.9})$$

And finally, the VSHs,  ${}^s \mathbf{F}_{\alpha, \mu\nu}^{(\iota)}(\mathbf{r})$ , will be given by the formulas below:

$${}^s \mathbf{F}_{M, \mu\nu}^{(\iota)}(\mathbf{r}) \triangleq \nabla \times \left[ \mathbf{r} {}^s \psi_{\mu\nu}^{(\iota)}(r, \theta, \phi) \right] = iz_\nu^{(\iota)}(kr) \mathbf{f}_{M, \mu\nu}(\hat{\mathbf{r}}), \quad (\text{B.10})$$

$$\begin{aligned} {}^s\mathbf{F}_{N,\mu\nu}^{(l)}(\mathbf{r}) &\triangleq \frac{1}{k} \nabla \times {}^s\mathbf{F}_{M,\mu\nu}^{(l)}(\mathbf{r}) \\ &= \hat{\mathbf{r}} \frac{v(v+1)}{kr} {}^s\psi_{\mu\nu}^{(l)}(r, \theta, \phi) + \tilde{z}_v^{(l)}(kr) \mathbf{f}_{N,\mu\nu}(\hat{\mathbf{r}}), \end{aligned} \quad (\text{B.11})$$

where:

$$\mathbf{f}_{M,\mu\nu}(\hat{\mathbf{r}}) = \gamma_{\mu\nu} \left[ \hat{\theta} \tau_{\mu\nu}^{(1)}(\theta) + i \hat{\phi} \tau_{\mu\nu}^{(2)}(\theta) \right] e^{i\mu\phi}, \quad (\text{B.12})$$

$$\mathbf{f}_{N,\mu\nu}(\hat{\mathbf{r}}) = \gamma_{\mu\nu} \left[ \hat{\theta} \tau_{\mu\nu}^{(2)}(\theta) + i \hat{\phi} \tau_{\mu\nu}^{(1)}(\theta) \right] e^{i\mu\phi}, \quad (\text{B.13})$$

$$\tilde{z}_v^{(l)}(x) = \frac{1}{x} \frac{\partial}{\partial x} [x z_v^{(l)}(x)], \quad (\text{B.14})$$

$$\tau_{\mu\nu}^{(1)}(\theta) = \mu \frac{P_v^\mu(\cos\theta)}{\sin\theta}, \quad (\text{B.15})$$

$$\tau_{\mu\nu}^{(2)}(\theta) = \frac{\partial P_v^\mu(\cos\theta)}{\partial \theta}. \quad (\text{B.16})$$

Having defined the above vector wave functions in the three coordinate systems, let us now give the formulas that expand the DGF into such eigenmodes. Avoiding the point singularity at  $\mathbf{r} = \mathbf{r}_0$ , i.e., the irrotational terms, the DGF can be expanded into a series of VPHs, VCHs, VSHs according to the following formulas [59]:

$$\begin{aligned} \vec{\mathbf{G}}(\mathbf{r}, \mathbf{r}_0) &\stackrel{\text{p}}{\equiv} \frac{i}{8\pi^2} \sum_{\alpha} \iint_{-\infty}^{+\infty} \frac{dk_x dk_y}{\sqrt{k^2 - k_x^2 - k_y^2}} \\ &\times \begin{cases} {}^p\mathbf{F}_{\alpha, k_x k_y}^{(-)}(\mathbf{r}) \otimes {}^p\mathbf{F}_{\alpha, -k_x -k_y}^{(+)}(\mathbf{r}_0), & z < z_0 \\ {}^p\mathbf{F}_{\alpha, k_x k_y}^{(+)}(\mathbf{r}) \otimes {}^p\mathbf{F}_{\alpha, -k_x -k_y}^{(-)}(\mathbf{r}_0), & z > z_0 \end{cases} \end{aligned} \quad (\text{B.17})$$

$$\begin{aligned} \vec{\mathbf{G}}(\mathbf{r}, \mathbf{r}_0) &\stackrel{\text{c}}{\equiv} \frac{i}{8\pi} \sum_{\mu, \alpha} (-1)^\mu \int_{-\infty}^{+\infty} dk_z \\ &\times \begin{cases} {}^c\mathbf{F}_{\alpha, \mu k_z}^{(1)}(\mathbf{r}) \otimes {}^c\mathbf{F}_{\alpha, -\mu -k_z}^{(3)}(\mathbf{r}_0), & \rho < \rho_0 \\ {}^c\mathbf{F}_{\alpha, \mu k_z}^{(3)}(\mathbf{r}) \otimes {}^c\mathbf{F}_{\alpha, -\mu -k_z}^{(1)}(\mathbf{r}_0), & \rho > \rho_0 \end{cases} \end{aligned} \quad (\text{B.18})$$

$$\begin{aligned} \vec{\mathbf{G}}(\mathbf{r}, \mathbf{r}_0) &\stackrel{\text{s}}{\equiv} ik \sum_{\nu, \mu, \alpha} (-1)^\mu \\ &\times \begin{cases} {}^s\mathbf{F}_{\alpha, \mu\nu}^{(1)}(\mathbf{r}) \otimes {}^s\mathbf{F}_{\alpha, -\mu\nu}^{(3)}(\mathbf{r}_0), & r < r_0 \\ {}^s\mathbf{F}_{\alpha, \mu\nu}^{(3)}(\mathbf{r}) \otimes {}^s\mathbf{F}_{\alpha, -\mu\nu}^{(1)}(\mathbf{r}_0), & r > r_0 \end{cases} \end{aligned} \quad (\text{B.19})$$

The last three formulas constitute explicit expressions of the series expansion of the DGF in Eq. (2) of the main text.

### Appendix C. Explicit expressions for the topological-skeleton-based representations of the scattered fields.

In this Appendix, we provide explicit expressions for the topological-skeleton-based representations of the scattered fields, as they are given by Eqs. (5) and (6) of the main text.

For 2D scatterers, i.e. for scatterers that have continuous translation symmetry along the z-axis, we can get the following representation of the scattered field as a series expansion of cylindrical waves distributed on top of the topological skeleton of the scatterer. By making use of Eq. (1) and the second branch of Eq. (B.18), we get the following expressions:

$$\begin{aligned} \mathbf{E}_{\text{sca}}(\mathbf{r}) &\stackrel{\text{c}}{\equiv} \sum_{\alpha, \mu} \int_{-\infty}^{+\infty} dk_z \int_C d\mathbf{r}_0 {}^c\mathcal{B}_{\alpha, \mu k_z}(\mathbf{r}_0) \\ &\times {}^c\mathbf{F}_{\alpha, \mu k_z}^{(3)}(\mathbf{r} - \mathbf{r}_\sigma(\mathbf{r}_0)), \text{ for } \mathbf{r} \in V_{\text{Sout}}, \end{aligned} \quad (\text{C.1})$$

with

$$\begin{aligned} {}^c\mathcal{B}_{\alpha, \mu k_z}(\mathbf{r}_0) &= \frac{i}{8\pi} (-1)^\mu \int_{-\infty}^{+\infty} dz_0 \times \\ &\left[ {}^c\mathbf{F}_{\alpha, -\mu -k_z}^{(1)}(\mathbf{r}_0 + z_0 \hat{\mathbf{z}} - \mathbf{r}_\sigma(\mathbf{r}_0)) \cdot [\hat{\mathbf{n}} \times \nabla \times \mathbf{E}_{\text{sca}}(\mathbf{r}_0 + z_0 \hat{\mathbf{z}})] \right. \\ &\left. + k {}^c\mathbf{F}_{\beta, -\mu -k_z}^{(1)}(\mathbf{r}_0 + z_0 \hat{\mathbf{z}} - \mathbf{r}_\sigma(\mathbf{r}_0)) \cdot [\hat{\mathbf{n}} \times \mathbf{E}_{\text{sca}}(\mathbf{r}_0 + z_0 \hat{\mathbf{z}})] \right]. \end{aligned} \quad (\text{C.2})$$

Note that here C is the contour of the cross-section of the scatterer across the  $z = 0$  plane, and  $\hat{\mathbf{n}}(\mathbf{r}_0)$  is the vector normal to the contour C, pointing outwards. Moreover, note that here  $\beta \neq \alpha$  and we made use of the property that the curl of a TE(TM) wave gives a TM(TE) wave multiplied by the wavenumber  $k$ . For finite dimensional representations, i.e. for a discretized topological skeleton, the above expressions take the following form:

$$\begin{aligned} \mathbf{E}_{\text{sca}}(\mathbf{r}) &\stackrel{\text{c}}{\equiv} \sum_{\alpha, \mu} \int_{-\infty}^{+\infty} dk_z \sum_{i=1}^N {}^c\mathcal{B}_{\alpha, \mu k_z, i} {}^c\mathbf{F}_{\alpha, \mu k_z}^{(3)}(\mathbf{r} - \mathbf{r}_i), \\ &\text{for } \sqrt{(x - x_i)^2 + (y - y_i)^2} > R_i, \quad \forall i, \end{aligned} \quad (\text{C.3})$$

with

$$\begin{aligned} {}^c\mathcal{B}_{\alpha, \mu k_z, i} &= \frac{i}{8\pi} (-1)^\mu \int_{C_i} d\mathbf{r}_0 \int_{-\infty}^{+\infty} dz_0 \\ &\times \left[ {}^c\mathbf{F}_{\alpha, -\mu -k_z}^{(1)}(\mathbf{r}_0 + z_0 \hat{\mathbf{z}} - \mathbf{r}_i) \cdot [\hat{\mathbf{n}} \times \nabla \times \mathbf{E}_{\text{sca}}(\mathbf{r}_0 + z_0 \hat{\mathbf{z}})] \right. \\ &\left. + k {}^c\mathbf{F}_{\beta, -\mu -k_z}^{(1)}(\mathbf{r}_0 + z_0 \hat{\mathbf{z}} - \mathbf{r}_i) \cdot [\hat{\mathbf{n}} \times \mathbf{E}_{\text{sca}}(\mathbf{r}_0 + z_0 \hat{\mathbf{z}})] \right]. \end{aligned} \quad (\text{C.4})$$

Note that here we use  $N$  centers (axis) of expansion that are centered at  $\mathbf{r}_i = x_i \hat{\mathbf{x}} + y_i \hat{\mathbf{y}}$ .  $C_i$  is the  $i$ -th segment of the contour C and  $R_i$  is the minimum radius of the circle centered at  $\mathbf{r}_i$  enclosing the segment  $C_i$ .

For 3D scatterers, we can get the following representation of the scattered field as a series expansion of spherical waves distributed on top of the topological skeleton of the scatterer. By making use of Eq. (1) and the second branch of Eq. (B.19) we get the following expressions:

$$\mathbf{E}_{\text{sca}}(\mathbf{r}) \stackrel{\text{s}}{\equiv} \sum_{\alpha, \mu, \nu} \int_S d^2\mathbf{r}_0 {}^s\mathcal{B}_{\alpha, \mu\nu}(\mathbf{r}_0) {}^s\mathbf{F}_{\alpha, \mu\nu}^{(3)}(\mathbf{r} - \mathbf{r}_\sigma(\mathbf{r}_0)), \text{ for } \mathbf{r} \in V_{\text{Sout}}, \quad (\text{C.5})$$

with

$$\begin{aligned} {}^s\mathcal{B}_{\alpha, \mu\nu}(\mathbf{r}_0) &= ik(-1)^\mu \\ &\times \left[ {}^s\mathbf{F}_{\alpha, -\mu\nu}^{(1)}(\mathbf{r}_0 - \mathbf{r}_\sigma(\mathbf{r}_0)) \cdot [\hat{\mathbf{n}} \times \nabla \times \mathbf{E}_{\text{sca}}(\mathbf{r}_0)] \right. \\ &\left. + k {}^s\mathbf{F}_{\beta, -\mu\nu}^{(1)}(\mathbf{r}_0 - \mathbf{r}_\sigma(\mathbf{r}_0)) \cdot [\hat{\mathbf{n}} \times \mathbf{E}_{\text{sca}}(\mathbf{r}_0)] \right]. \end{aligned} \quad (\text{C.6})$$

For finite dimensional representations, i.e. for a discretized topological skeleton, the above expressions take the following form:

$$\begin{aligned} \mathbf{E}_{\text{sca}}(\mathbf{r}) &\stackrel{\text{s}}{\equiv} \sum_{\alpha, \mu, \nu} \sum_{i=1}^N {}^s\mathcal{B}_{\alpha, \mu\nu, i} {}^s\mathbf{F}_{\alpha, \mu\nu}^{(3)}(\mathbf{r} - \mathbf{r}_i), \\ &\text{for } |\mathbf{r} - \mathbf{r}_i| > R_i, \quad \forall i, \end{aligned} \quad (\text{C.7})$$

with

$$\begin{aligned} {}^s\mathcal{B}_{\alpha, \mu\nu, i} &= ik(-1)^\mu \int_{S_i} d^2\mathbf{r}_0 \\ &\times \left[ {}^s\mathbf{F}_{\alpha, -\mu\nu}^{(1)}(\mathbf{r}_0 - \mathbf{r}_i) \cdot [\hat{\mathbf{n}} \times \nabla \times \mathbf{E}_{\text{sca}}(\mathbf{r}_0)] \right. \\ &\left. + k {}^s\mathbf{F}_{\beta, -\mu\nu}^{(1)}(\mathbf{r}_0 - \mathbf{r}_i) \cdot [\hat{\mathbf{n}} \times \mathbf{E}_{\text{sca}}(\mathbf{r}_0)] \right]. \end{aligned} \quad (\text{C.8})$$

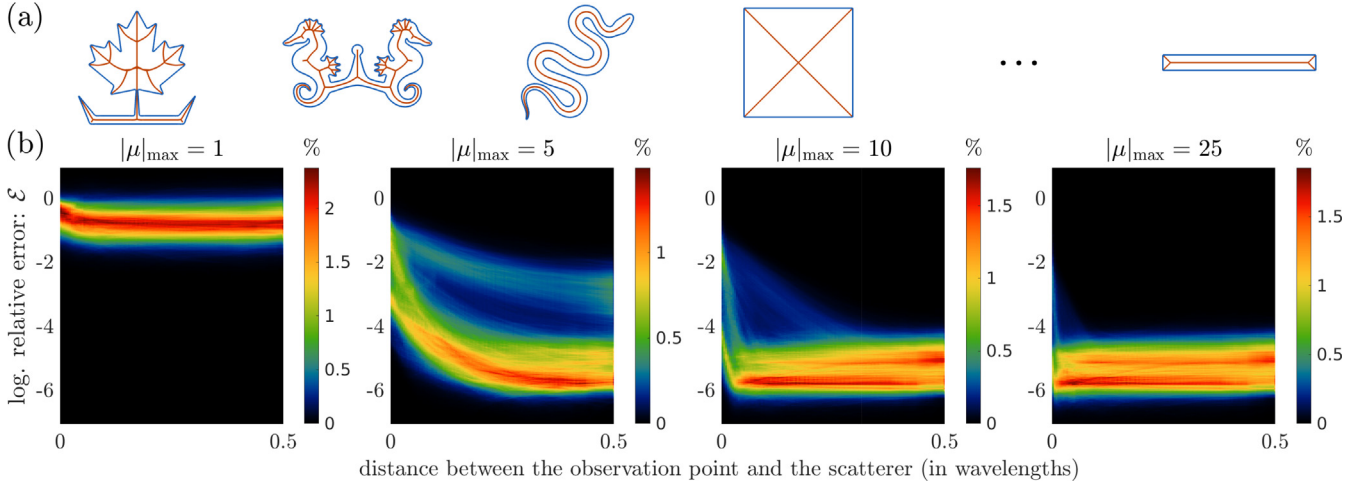


**Fig. D.1.** Statistical analysis of the convergence among several instances of 2D scatterers with varying geometry [illustrated with blue color in (a)], illuminated by TE-polarized plane waves propagating along varying directions on the  $xy$ -plane. In (b), we plot the statistics of the log. relative errors  $\mathcal{E}(\mathbf{r})$  recorded for the topological-skeleton-based representations [the topological skeleton of the 2D scatterers is illustrated with red color in (a)], as a function of the distance (in terms of free space wavelengths) between the observation point and the surface of the scatterer, and for varying truncation orders of the multipolar series ( $|\mu|_{\max}$ ). The angle of the illuminating plane waves is varied with a step of  $5^\circ$  (for all non-trivial excitation angles with respect to the geometry of the scatterer). The scatterers are again considered to be inscribed inside a circle of radius half the free space wavelength. They are made of a material of refractive index  $n = 3.477$  and embedded in free space. Eleven rectangular scatterers are considered with varying aspect ratios from one to ten. The surface and the topological skeleton of each scatterer are finely discretized using a large number of 12,000 points. We can observe that a smaller optical distance between the observation point and the scatterer generally requires a larger number of multipoles for sufficient convergence. Note, also, the different rates of convergence that we characteristically can observe, e.g., in the case of  $|\mu|_{\max} = 5$ , which is indicative of the additional role of the distance between the centers of multipolar expansion and the surface of the scatterer (or, to be more precise, the singularities of the analytic continuation of the fields that they represent) when it comes to the convergence of the multipolar-series representation of the fields; a larger such distance also requires a larger number of multipoles for convergence. (For interpretation of the references to colour in this figure legend, the reader is referred to the web version of this article.)

#### Appendix D. On the convergence of representations of the scattered field based on a multipolar series

In this Appendix, we provide with the following three figures some extra material that supports our remarks in the main text regarding the convergence of representations of the scattered field based on multipolar series.

In the first figure (Fig. D.1), we perform a statistical analysis of the convergence among several instances of 2D scatterers with varying geometry, illuminated by TE-polarized plane waves propagating along varying directions. There, we plot the statistics of the log. relative errors recorded for the topological-skeleton-based representations, as a function of the distance between the observation point and the surface of the scatterer. We observe that there is a slower convergence rate recorded for smaller distances. The closer the observation point to the surface of the scatterer, the larger the number of multipoles needed for convergence. However, it is also

observed that the rate of such convergence is not unique. As discussed already, the convergence also depends on the distance between the multipolar center of expansion and the surface of the scatterer. For the cases of scatterers where such distance between the topological skeleton and the surface of the scatterer becomes large (like for rectangular scatterers of low aspect ratio), we observe a slower convergence rate.

In the second figure (Fig. D.2), we demonstrate the rate of convergence for the case of a cylinder illuminated by a dipolar emitter placed in close proximity on top of it. The emitter is known to induce an image singularity in the analytic continuation of the scattered fields of the cylinder at a small distance from its surface. In this case, we observe a slower convergence rate for the topological-skeleton-based representation of the scattered field in multipolar series. Although, theoretically, we can still achieve convergence all over the near-field region, we observe that a larger number of multipoles are needed for convergence. That holds es-

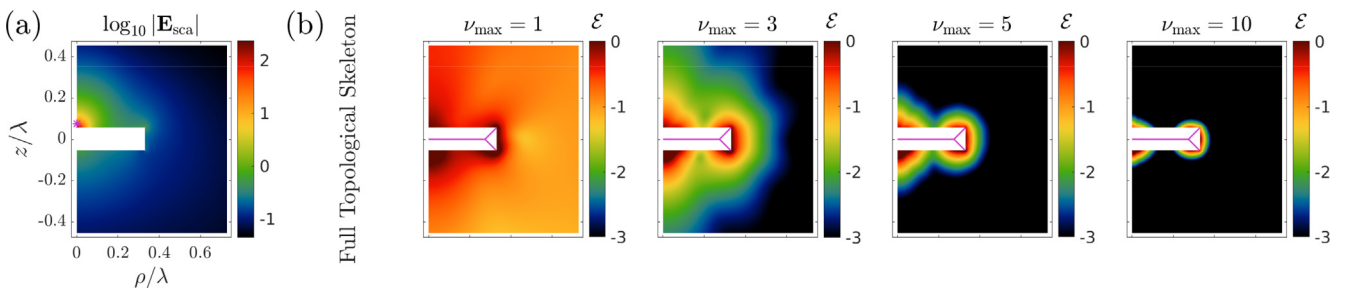


**Fig. D.2.** Checking the convergence of the topological-skeleton-based representation of a radiating field with a singularity located closely to the physical domain. A cylinder with axial symmetry to the  $z$ -axis and with an aspect ratio of six, inscribed inside a sphere of radius one third of the free space wavelength  $\lambda$ , made of a material of refractive index  $n = 3.477$  and embedded in free space, is excited by a  $z$ -oriented electric dipole placed at a distance of  $\lambda/50$  on top of the disk [illustrated with a magenta star in (a)]. In (a), we plot the logarithm of the norm of the scattered by the disk field upon such an excitation. We can observe the strong gradients of the field. In (b), we plot maps of the log. relative error  $\mathcal{E}(\mathbf{r})$  for the topological-skeleton-based representation of the fields for increasing truncation orders of the multipolar series. The magenta line denotes the topological skeleton of the cylinder. Here we use 8,250 unevenly distributed (we considered a denser discretization at the region of strong gradients of the incident field) points for the fine discretization of both the surface of the cylinder and the topological skeleton over the meridian plane. We observe that, in this case, the convergence is relatively poorer compared with what we observed before due to the strongly singular radiated fields.

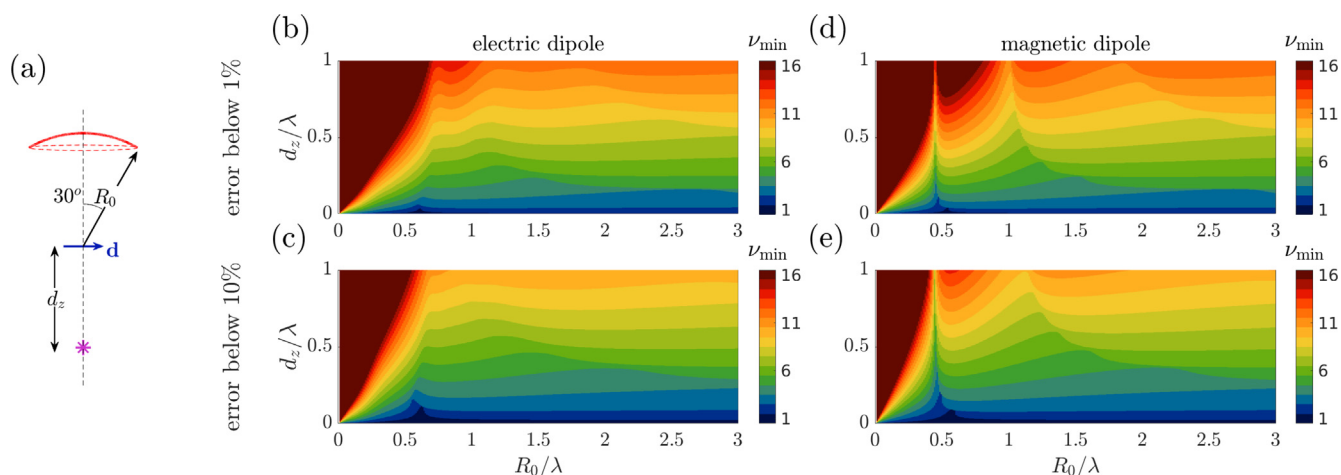


**Fig. D.3.** Study of the number of multipoles required for the reconstruction of the fields radiated by a dipolar emitter in free space, as a function of 1) the optical distance between the emitter and the observation point ( $R_0/\lambda$ ), and 2) the optical distance between the emitter and a center of multipolar expansion that is used to represent the radiation of the emitter ( $d_z/\lambda$ ). a) The geometry of the problem. The magenta star indicates the position of the multipolar expansion. The blue vector indicates the position and orientation of the dipolar emitter. The red curve indicates the cross-section of a spherical cap over which we calculate the convergence of the representation of the radiated fields. b-e) Maps of the minimum multipolar order needed ( $\nu_{\min}$ ) to achieve an average error below either 1% (b,d), or 10% (c,e), for the case of either an electric dipole (b,c) or a magnetic dipole (d,e) emitter. We observe that, as  $d_z/\lambda$  increases and  $R_0/\lambda$  decreases, the minimum number of multipoles needed for convergence increases. Moreover, for a fixed value of  $d_z/\lambda$ , the number of multipoles needed for convergence remains practically invariant to  $R_0/\lambda$  beyond some value of  $R_0/\lambda$ . (For interpretation of the references to colour in this figure legend, the reader is referred to the web version of this article.)

pecially in the region in the vicinity of the image singularity inside the disk, which locally induces strong gradients to the near-fields.

Finally, in the third figure (Fig. D.3), we demonstrate the number of multipoles needed to achieve convergence for the reconstruction of the fields radiated by a dipolar emitter in free space as a function of 1) the optical distance between the emitter and the observation point ( $R_0/\lambda$ ), and 2) the optical distance between the emitter and a center of multipolar expansion that is used to represent the radiation of the emitter ( $d_z/\lambda$ ). The fields radiated by the emitter have a singularity at its position. There, we observe that: 1) the larger the optical distance  $d_z/\lambda$ , the larger the number of multipoles needed for convergence, and 2) the larger the distance  $R_0/\lambda$ , the smaller the number of multipoles that are needed for convergence. Note that, after some value of  $R_0/\lambda$ , as we move away from the singularity, i.e., as we move away from the near-field region of the radiated fields, the number of multipoles needed for convergence (for a particular  $d_z/\lambda$ ), remains practically unchanged concerning  $R_0/\lambda$ .

## References

- [1] Rayleigh L. On the dynamical theory of gratings. *Proc R Soc London SerA* 1907;79(532):399–416. <http://www.jstor.org/stable/92655>.
- [2] Millar RF. On the Rayleigh assumption in scattering by a periodic surface. *Math Proc Cambridge Philos Soc* 1969;65(3):773–91. doi:10.1017/S0305004100003613.
- [3] Millar RF. The Rayleigh hypothesis and a related least-squares solution to scattering problems for periodic surfaces and other scatterers. *Radio Sci* 1973;8(8–9):785–96. doi:10.1029/RS008i008p00785.
- [4] TBates R. Analytic constraints on electromagnetic field computations. *IEEE Trans Microw Theory Tech* 1975;23(8):605–23. doi:10.1109/TMTT.1975.1128639.
- [5] van den Berg PM, Fokkema JT. The Rayleigh hypothesis in the theory of reflection by a grating. *J Opt Soc Am* 1979;69(1):27–31. doi:10.1364/JOSA.69.000027.
- [6] van den Berg PM, Fokkema JT. The Rayleigh hypothesis in the theory of diffraction by a perturbation in a plane surface. *Radio Sci* 1980;15(4):723–32. doi:10.1029/RS015i004p00723.
- [7] Maystre D, Cadilhac M. Singularities of the continuation of fields and validity of Rayleigh's hypothesis. *J Math Phys* 1985;26(9):2201–4. doi:10.1063/1.526847.
- [8] Burrows M. Equivalence of the rayleigh solution and the extended-boundary-condition solution for scattering problems. *Electron Lett* 1969;5:277–8. [https://digital-library.theiet.org/content/journals/10.1049/el\\_19690210](https://digital-library.theiet.org/content/journals/10.1049/el_19690210).
- [9] Kyurkchan AG, Sternin BY, Shatalov VE. Singularities of continuation of wave fields. *Phys Usp* 1996;39(12):1221–42. doi:10.1070/PU1996v039n12abeh000184.
- [10] Kyurkchan A, Smirnova N. Mathematical modeling in diffraction theory: based on a priori information on the analytical properties of the solution. Elsevier Science; 2015. ISBN 9780128037485. <https://books.google.de/books?id=gHy8BwAAQBA>.
- [11] Voronovich AG. *Rayleigh hypothesis*. Boston, MA: Springer US; 2007. p. 93–105.
- [12] Kalhor H. Numerical evaluation of Rayleigh hypothesis for analyzing scattering from corrugated gratings—TE polarization. *IEEE Trans Antennas Propag* 1976;24(6):884–9. doi:10.1109/TAP.1976.1141432.
- [13] Soto-Crespo JM, Nieto-Vesperinas M, Friberg AT. Scattering from slightly rough random surfaces: a detailed study on the validity of the small perturbation method. *J Opt Soc Am A* 1990;7(7):1185–201. doi:10.1364/JOSA.7.001185.
- [14] Christiansen S, Kleinman R. On a misconception involving point collocation and the Rayleigh hypothesis. *IEEE Trans Antennas Propag* 1996;44(10):1309–16. doi:10.1109/8.537324.
- [15] Zaridze R, Bit-Babik G, Tavzarashvili K, Economou D, Uzunoglu N. Wave field singularity aspects in large-size scatterers and inverse problems. *IEEE Trans Antennas Propag* 2002;50(1):50–8. doi:10.1109/8.992561.
- [16] Watanabe T, Choyal Y, Minami K, Granatstein VL. Range of validity of the Rayleigh hypothesis. *Phys Rev E* 2004;69:056606. doi:10.1103/PhysRevE.69.056606.
- [17] Tishchenko AV. Numerical demonstration of the validity of the Rayleigh hypothesis. *Opt Express* 2009;17(19):17102–17. doi:10.1364/OE.17.017102.
- [18] Petoev I, Tabatadze V, Kakulia D, Zaridze R. About scattered field's singularities and Rayleigh hypothesis. In: 2012 XVIIIth International Seminar/Workshop on Direct and Inverse Problems of Electromagnetic and Acoustic Wave Theory - (DIPED); 2012. p. 17–22.
- [19] Martin PA. Two-dimensional acoustic scattering, conformal mapping, and the Rayleigh hypothesis. *J Acoust Soc Am* 2012;132(4):2184–8. doi:10.1121/1.4747004.
- [20] Rother T, Kahnert M. *The Rayleigh hypothesis*. Berlin, Heidelberg: Springer Berlin Heidelberg; 2014. p. 171–201. ISBN 978-3-642-36745-8
- [21] Antonov AA, Gorkunov MV. Corrugated silicon metasurface optimized within the Rayleigh hypothesis for anomalous refraction at large angles. *J Opt Soc Am B* 2019;36(8):2118–25. doi:10.1364/JOSAB.36.002118.
- [22] Rother T, Hawkins SC. Notes on Rayleigh's hypothesis and the extended boundary condition method. *J Acoust Soc Am* 2021;149(4):2179–88. doi:10.1121/1.0003958.
- [23] Auguie B, Somerville WRC, Roache S, Ru ECL. Numerical investigation of the Rayleigh hypothesis for electromagnetic scattering by a particle. *J Opt* 2016;18(7):075007. doi:10.1088/2040-8978/18/7/075007.
- [24] Schebarchov D, Ru ECL, Grand J, Auguie B. Mind the gap: testing the rayleigh hypothesis in t-matrix calculations with adjacent spheroids. *Opt Express* 2019;27(24):35750–60. doi:10.1364/OE.27.035750.
- [25] Tittel A, Leitis A, Liu M, Yesilkoy F, Choi D-Y, Neshev DN, Kivshar YS, Altug H. Imaging-based molecular barcoding with pixelated dielectric metasurfaces. *Science* 2018;360(6393):1105–9. doi:10.1126/science.aas9768.
- [26] Scott P, Garcia-Santiago X, Beutel D, Rockstuhl C, Wegener M, Fernandez-Corbaton I. On enhanced sensing of chiral molecules in optical cavities. *Appl Phys Rev* 2020;7(4):041413. doi:10.1063/5.0025006.
- [27] Donie YJ, Smeets M, Egel A, Lentz F, Preinfalk JB, Mertens A, Smirnov V, Lemmer U, Bittkau K, Gomard G. Light trapping in thin film silicon solar cells via phase separated disordered nanopillars. *Nanoscale* 2018;10:6651–9. doi:10.1039/C8NR00455B.

- [28] Piechulla PM, Slivina E, Bätzner D, Fernandez-Corbaton I, Dhawan P, Wehrspohn RB, Sprafke AN, Rockstuhl C. Antireflective Huygens' metasurface with correlated disorder made from high-index disks implemented into silicon heterojunction solar cells. *ACS Photonics* 2021;8(12):3476–85. doi:10.1021/acsp Photonics.1c00601.
- [29] Pratesi F, Burresti M, Riboli F, Vynck K, Wiersma DS. Disordered photonic structures for light harvesting in solar cells. *Opt Express* 2013;21(S3):A460–8. doi:10.1364/OE.21.00A460.
- [30] Vynck K, Burresti M, Riboli F, Wiersma DS. Photon management in two-dimensional disordered media. *Nat Mater* 2012;11(12):1017–22. doi:10.1038/nmat3442.
- [31] Gomard G, Preinfalk JB, Egel A, Lemmer U. Photon management in solution-processed organic light-emitting diodes: a review of light outcoupling micro- and nanostructures. *J Photonics Energy* 2016;6(3):030901. doi:10.1117/1.JPE.6.030901.
- [32] Arslan D, Rahimzadegan A, Fasold S, Falkner M, Zhou W, Kroychuk M, Rockstuhl C, Pertsch T, Staudte I. Toward perfect optical diffusers: dielectric Huygens metasurfaces with critical positional disorder. *Adv Mater* 2022;34(5):2105868. doi:10.1002/adma.202105868.
- [33] Zhelyeznyakov MV, Zhan A, Majumdar A. Design and optimization of ellipsoid scatterer-based metasurfaces via the inverse T-matrix method. *OSA Continuum* 2020;3(1):89–103. doi:10.1364/OE.376537.
- [34] Kim J, Yang Y, Badloe T, Kim I, Yoon G, Rho J. Geometric and physical configurations of meta-atoms for advanced metasurface holography. *InfoMat* 2021;3(7):739–54. doi:10.1002/infm2.12191.
- [35] Stefanou N, Yannopapas V, Modinos A. MULTEM 2: a new version of the program for transmission and band-structure calculations of photonic crystals. *Comput Phys Commun* 2000;132(1):189–96. doi:10.1016/S0010-4655(00)00131-4.
- [36] Egel A, Pattelli L, Mazzamuto G, Wiersma DS, Lemmer U. CELES: CUDA-accelerated simulation of electromagnetic scattering by large ensembles of spheres. *J Quant Spectrosc Radiat Transf* 2017a;199:103–10. doi:10.1016/j.jqsrt.2017.05.010.
- [37] Egel A, Czajkowski KM, Theobald D, Ladutenko K, Kuznetsov AS, Pattelli L. SMUTHI: a python package for the simulation of light scattering by multiple particles near or between planar interfaces. *J Quant Spectrosc Radiat Transf* 2021;273:107846. doi:10.1016/j.jqsrt.2021.107846.
- [38] Theobald D, Beutel D, Borgmann L, Mescher H, Gomard G, Rockstuhl C, Lemmer U. Simulation of light scattering in large, disordered nanostructures using a periodic T-matrix method. *J Quant Spectrosc Radiat Transf* 2021;272:107802. doi:10.1016/j.jqsrt.2021.107802.
- [39] Bertrand M, Devilez A, Hugonin J-P, Lalanne P, Vynck K. Global polarizability matrix method for efficient modeling of light scattering by dense ensembles of non-spherical particles in stratified media. *J Opt Soc Am A* 2020;37(1):70–83. doi:10.1364/JOSAA.37.000070.
- [40] Skarda J, Trivedi R, Su L, Ahmad-Stein D, Kwon H, Han S, Fan S, Vučković J. Low-overhead distribution strategy for simulation and optimization of large-area metasurfaces. *npj Comput Mater* 2022;8(1):78. doi:10.1038/s41524-022-00774-y.
- [41] Beutel D, Groner A, Rockstuhl C, Fernandez-Corbaton I. Efficient simulation of biperiodic, layered structures based on the T-matrix method. *J Opt Soc Am B* 2021;38(6):1782–91. doi:10.1364/JOSAB.419645.
- [42] Rahimzadegan A, Karamanos TD, Alaei R, Lamprianidis AG, Beutel D, Boyd RW, Rockstuhl C. A comprehensive multipolar theory for periodic metasurfaces. *Adv Opt Mater* 2022;10(10):2102059. doi:10.1002/adom.202102059.
- [43] Wiecha PR. pyGDM—a python toolkit for full-field electro-dynamical simulations and evolutionary optimization of nanostructures. *Comput Phys Commun* 2018;233:167–92. doi:10.1016/j.cpc.2018.06.017.
- [44] Mie G. Beitrage zur optik trber medien, speziell kolloidaler metallungen. *Ann Phys* 1908;330(3):377–445. doi:10.1002/andp.19083300302.
- [45] Fruhnert M, Fernandez-Corbaton I, Yannopapas V, Rockstuhl C. Computing the T-matrix of a scattering object with multiple plane wave illuminations. *Beilstein J Nanotechnol* 2017;8:614–26. doi:10.3762/bjnano.8.66.
- [46] Demésy G, Auger J-C, Stout B. Scattering matrix of arbitrarily shaped objects: combining finite elements and vector partial waves. *J Opt Soc Am A* 2018;35(8):1401–9. doi:10.1364/JOSAA.35.001401.
- [47] Wriedt T. Generalized multipole techniques for electromagnetic and light scattering. Elsevier Science; 1999. ISSN: ISBN 9780080532370, <https://books.google.de/books?id=I9613oULCkwC>.
- [48] Wriedt T, Eremin Y. The generalized multipole technique for light scattering: recent developments. Springer Series on Atomic, Optical, and Plasma Physics. Springer International Publishing; 2018. ISBN 9783319748900, [https://books.google.de/books?id=\\_49QDwAAQBAJ](https://books.google.de/books?id=_49QDwAAQBAJ).
- [49] Doicu A, Wriedt T, Eremin Y. Light scattering by systems of particles: null-field method with discrete sources: theory and programs. Springer Series in Optical Sciences. Springer Berlin Heidelberg; 2006. ISBN 9783540336976, <https://books.google.de/books?id=NXX7BQAAQBAJ>.
- [50] Mishchenko M, Andrew A Laci M, Travis L, Laci A. Scattering, absorption, and emission of light by small particles. Cambridge University Press; 2002. ISBN 9780521782524, [https://books.google.de/books?id=i6r1YFyK\\_g8C](https://books.google.de/books?id=i6r1YFyK_g8C).
- [51] Pulbere S, Wriedt T. Light scattering by cylindrical fibers with high aspect ratio using the null-field method with discrete sources. *Particle Particle Syst. Character.* 2004;21(3):213–18. doi:10.1002/ppsc.200400864.
- [52] Wriedt T. Review of the null-field method with discrete sources. *J Quant Spectrosc Radiat Transf* 2007;106(1):535–545. doi:10.1016/j.jqsrt.2007.01.043. IX Conference on Electromagnetic and Light Scattering by Non-Spherical Particles
- [53] Doicu A. Acoustic and electromagnetic scattering analysis using discrete sources. 2000. 10.1016/B978-012219740-6/50000-9
- [54] Eremin J, Orlov N, Rozenberg V. Scattering by non-spherical particles. *Comput Phys Commun* 1994;79(2):201–14. doi:10.1016/0010-4655(94)90068-X.
- [55] Moreno E, Erni D, Hafner C, Vahldieck R. Multiple multipole method with automatic multipole setting applied to the simulation of surface plasmons in metallic nanostructures. *J Opt Soc Am A* 2002;19(1):101–11. doi:10.1364/JOSAA.19.001011.
- [56] Blum H. A transformation for extracting new descriptors of shape. MIT Press; 1967. <https://books.google.de/books?id=0Jl5zQEACAAJ>.
- [57] Saha P, Borgefors G, di Baja G. Skeletonization: theory, methods and applications. Elsevier Science; 2017. ISBN 9780081012925, <https://books.google.de/books?id=x7oIdgAAQBAJ>.
- [58] Stratton JA, Chu LJ. Diffraction theory of electromagnetic waves. *Phys Rev* 1939;56:99–107. doi:10.1103/PhysRev.56.99.
- [59] Tai C, Antennas I, Society P, Theory IM, Society T. Dyadic green functions in electromagnetic theory. IEEE Press Publication Series. IEEE Press; 1994. ISBN 9780780304499, <https://books.google.de/books?id=wiNRAAAAMAAJ>.
- [60] Morse P, Feshbach H. Methods of theoretical physics. International series in pure and applied physics. McGraw-Hill; 1953. <https://books.google.de/books?id=I8ENAAIAAJ>.
- [61] Miller W. Symmetry and separation of variables. Encyclopedia of Mathematics and its Applications. Cambridge University Press; 2012. ISBN 9780521177399, <https://books.google.de/books?id=ct6iSgAACAAJ>.
- [62] Egel A, Theobald D, Donie Y, Lemmer U, Gomard G. Light scattering by oblate particles near planar interfaces: on the validity of the t-matrix approach. *Opt Express* 2016;24(22):25154–68. doi:10.1364/OE.24.025154.
- [63] Theobald D, Egel A, Gomard G, Lemmer U. Plane-wave coupling formalism for t-matrix simulations of light scattering by nonspherical particles. *Phys Rev A* 2017;96:033822. doi:10.1103/PhysRevA.96.033822.
- [64] Egel A, Eremin Y, Wriedt T, Theobald D, Lemmer U, Gomard G. Extending the applicability of the T-matrix method to light scattering by flat particles on a substrate via truncation of sommerfeld integrals. *J Quant Spectrosc Radiat Transf* 2017b;202:279–285. doi:10.1016/j.jqsrt.2017.08.016.
- [65] Martin T. T-matrix method for closely adjacent obstacles. *J Quant Spectrosc Radiat Transf* 2019;234:40–46. doi:10.1016/j.jqsrt.2019.06.001.
- [66] Tsitsas NL, Zouros GP, Fikioris G, Leviatan Y. On methods employing auxiliary sources for 2-D electromagnetic scattering by noncircular shapes. *IEEE Trans Antennas Propag* 2018;66(10):5443–52. doi:10.1109/TAP.2018.2855963.
- [67] Zaridze R, Jobava R, Bit-Banik G, Karkasbadze D, Economou D, Uzunoglu N. The method of auxiliary sources and scattered field singularities (caustics). *J Electromagn Waves Appl* 1998;12(11):1491–507. doi:10.1163/15693998X00430.
- [68] Kklamani DI, Anastassi HT. Aspects of the method of auxiliary sources (MAS) in computational electromagnetics. *IEEE Antennas Propag Mag* 2002;44(3):48–64. doi:10.1109/MAP.2002.1028734.
- [69] Kern AM, Martin OJF. Surface integral formulation for 3D simulations of plasmonic and high permittivity nanostructures. *J Opt Soc Am A* 2009;26(4):732–40. doi:10.1364/JOSAA.26.000732.
- [70] Tagliasacchi A, Delame T, Spagnuolo M, Amenta N, Telea A. 3D skeletons: a state-of-the-art report. *Comput Graphics Forum* 2016;35(2):573–97. doi:10.1111/cgf.12865.
- [71] Sun F, Choi Y, Yu Y, Wang W. Medial meshes a compact and accurate representation of medial axis transform. *IEEE Trans Vis Comput Graph* 2016;22:1278–90.
- [72] Zou JJ, Chang H-H, Yan H. A new skeletonization algorithm based on constrained Delaunay triangulation. In: ISSPA '99: Proceedings of the Fifth International Symposium on Signal Processing and its Applications (IEEE Cat. No.99EX359), vol. 2; 1999. p. 927–30. doi:10.1109/ISSPA.1999.815823.
- [73] Burger S, Zschiedrich L, Pomplun J, Schmidt F. JCMsuite: an adaptive FEM solver for precise simulations in nano-optics. In: Integrated Photonics and Nanophotonics Research and Applications. Optica Publishing Group; 2008. p. ITuE4. doi:10.1364/IPNRA.2008.ITuE4.
- [74] Barnett A, Betcke T. Stability and convergence of the method of fundamental solutions for Helmholtz problems on analytic domains. *J Comput Phys* 2008;227(14):7003–26. doi:10.1016/j.jcp.2008.04.008.
- [75] Lakhtakia A, Iskander M, Durney C. An iterative extended boundary condition method for solving the absorption characteristics of lossy dielectric objects of large aspect ratios. *IEEE Trans Microw Theory Tech* 1983;31(8):640–7. doi:10.1109/TMTT.1983.1131562.
- [76] Novotny L, Hecht B. Principles of nano-optics. 2nd ed. Cambridge University Press; 2012. doi:10.1017/CBO9780511794193.